Zhu, Z., S. Piao, R.B. Myneni, M. Huang, Z. Zeng, J.G. Canadell, P. Ciais, S. Sitch, P. Friedlingstein, A. Arneth, C. Cao, L. Cheng, E. Kato, C. Koven, Y. Li, X. Lian, Y. Liu, R. Liu, J. Mao, Y. Pan, S. Peng, J. Penuelas, B. Poulter, T.A.M. Pugh, B.D. Stocker, N. Viovy, X. Wang, Y. Wang, Z. Xiao, H. Yang, S. Zaehle, and N. Zeng, 2016: Greening of the Earth and its drivers. *Nature Climate Change,* **6,** 791-795. http://dx.doi.org/10.1038/nclimate3004

Zunz, V., H. Goosse, and F. Massonnet, 2013: How does internal variability influence the ability of CMIP5 models to reproduce the recent trend in Southern Ocean sea ice extent? *The Cryosphere,* **7,** 451-468. http://dx.doi.org/10.5194/tc-7-451-2013

FINAL DRAFT

2. Physical Drivers of Climate Change

Key Findings

1. Human activities continue to significantly affect Earth's climate by altering factors that change its radiative balance. These factors, known as radiative forcings, include changes in greenhouse gases, small airborne particles (aerosols), and the reflectivity of the Earth's surface. In the industrial era, human activities have been, and are increasingly, the dominant cause of climate warming. The increase in radiative forcing due to these activities has far exceeded the relatively small net increase due to natural factors, which include changes in energy from the sun and the cooling effect of volcanic eruptions. (*Very high confidence*)

2. Aerosols caused by human activity play a profound and complex role in the climate system through radiative effects in the atmosphere and on snow and ice surfaces and through effects on cloud formation and properties. The combined forcing of aerosol–radiation and aerosol–cloud interactions is negative (cooling) over the industrial era (*high confidence*), offsetting a substantial part of greenhouse gas forcing, which is currently the predominant human contribution. The magnitude of this offset, globally averaged, has declined in recent decades, despite increasing trends in aerosol emissions or abundances in some regions (*medium* to *high confidence*)

3. The interconnected Earth–atmosphere–ocean system includes a number of positive and negative feedback processes that can either strengthen (positive feedback) or weaken (negative feedback) the system's responses to human and natural influences. These feedbacks operate on a range of timescales from very short (essentially instantaneous) to very long (centuries). Global warming by net radiative forcing over the industrial era includes a substantial amplification from these feedbacks (approximately a factor of three) (*high confidence*). While there are large uncertainties associated with some of these feedbacks, the net feedback effect over the industrial era has been positive (amplifying warming) and will continue to be positive in coming decades (*Very high confidence*).

2.0 Introduction

Earth's climate is undergoing substantial change due to anthropogenic activities (Ch. 1: Our Globally Changing Climate). Understanding the causes of past and present climate change and confidence in future projected changes depend directly on our ability to understand and model the physical drivers of climate change (Clark et al. 2016). Our understanding is challenged by the complexity and interconnectedness of the components of the climate system (that is, the atmosphere, land, ocean, and cryosphere). This chapter lays out the foundation of climate change by describing its physical drivers, which are primarily associated with atmospheric composition (gases and aerosols) and cloud effects. We describe the principle radiative forcings and the variety of feedback responses which serve to amplify these forcings.

FINAL DRAFT

2.1 Earth's Energy Balance and the Greenhouse Effect

The temperature of the Earth system is determined by the amounts of incoming (short-wavelength) and outgoing (both short- and long-wavelength) radiation. In the modern era, radiative fluxes are well-constrained by satellite measurements (Figure 2.1). About a third (29.4%) of incoming, short-wavelength energy from the sun is reflected back to space and the remainder is absorbed by the Earth system. The fraction of sunlight scattered back to space is determined by the reflectivity (albedo) of clouds, land surfaces (including snow and ice), oceans, and particles in the atmosphere. The amount and albedo of clouds, snow cover, and ice cover are particularly strong determinants of the amount of sunlight reflected back to space because their albedos are much higher than that of land and oceans.

In addition to reflected sunlight, Earth loses energy through infrared (long-wavelength) radiation from the surface and atmosphere. Greenhouse gases (GHGs) in the atmosphere absorb most of this radiation, leading to a warming of the surface and atmosphere. Figure 2.1 illustrates the importance of greenhouse gases in the energy balance of the Earth system. The naturally occurring GHGs in Earth's atmosphere—principally water vapor and carbon dioxide—keep the near-surface air temperature about 60°F (33°C) warmer than it would be in their absence, assuming albedo is held constant (Lacis et al. 2010). Geothermal heat from Earth's interior, direct heating from energy production, and frictional heating through tidal flows also contribute to the amount of energy available for heating the Earth's surface and atmosphere, but their total contribution is an extremely small fraction (< 0.1%) of that due to net solar (shortwave) and infrared (longwave) radiation (e.g., see Davies and Davies 2010; Flanner 2009; Munk and Wunsch 1998, where these forcings are quantified).

[INSERT FIGURE 2.1 HERE]

Thus, Earth's equilibrium temperature in the modern era is controlled by a short list of factors: incoming sunlight, absorbed and reflected sunlight, emitted infrared radiation, and infrared radiation absorbed and re-emitted in the atmosphere, primarily by GHGs. Changes in these factors affect Earth's radiative balance and therefore its climate, including but not limited to the average, near-surface air temperature. Anthropogenic activities have changed Earth's radiative balance and its albedo by adding GHGs, particles (aerosols), and aircraft contrails to the atmosphere, and through land-use changes. Changes in the radiative balance (or forcings) produce changes in temperature, precipitation, and other climate variables through a complex set of physical processes, many of which are coupled (Figure 2.2). These changes, in turn, trigger feedback processes which can further amplify and/or dampen the changes in radiative balance (Sections 2.5 and 2.6).

In the following sections, the principal components of the framework shown in Figure 2.2 are described. Climate models are structured to represent these processes; climate models and their components and associated uncertainties, are discussed in more detail in Chapter 4: Projections.

FINAL DRAFT

[INSERT FIGURE 2.2 HERE]

The processes and feedbacks connecting changes in Earth's radiative balance to a climate response (Figure 2.2) operate on a large range of timescales. Reaching an equilibrium temperature distribution in response to anthropogenic activities takes decades or longer because some components of the Earth system—in particular the oceans and cryosphere—are slow to respond due to their large thermal masses and the long timescale of circulation between the ocean surface and the deep ocean. Of the substantial energy gained in the combined ocean–atmosphere system over the previous four decades, over 90% of it has gone into ocean warming (Rhein et al. 2013; see Box 3.1 Fig 1). Even at equilibrium, internal variability in Earth's climate system causes limited annual- to decadal-scale variations in regional temperatures and other climate parameters that do not contribute to long-term trends. For example, it is *likely* that natural variability has contributed between –0.18°F (–0.1°C) and 0.18°F (0.1°C) to changes in surface temperatures from 1951 to 2010; by comparison, anthropogenic GHGs have *likely* contributed between 0.9°F (0.5°C) and 2.3°F (1.3°C) to observed surface warming over this same period (Bindoff et al. 2013). Due to these longer timescale responses and natural variability, changes in Earth's radiative balance are not realized immediately as changes in climate, and even in equilibrium there will always be variability around mean conditions.

2.2 Radiative Forcing (RF) and Effective Radiative Forcing (ERF)

Radiative forcing (RF) is widely used to quantify a radiative imbalance in Earth's atmosphere resulting from either natural changes or anthropogenic activities over the industrial era. It is expressed as a change in net radiative flux (W/m^2) either at the tropopause or top of the atmosphere (Myhre et al. 2013), with the latter nominally defined at 20 km altitude to optimize observation/model comparisons (Loeb et al. 2002). The instantaneous RF is defined as the immediate change in net radiative flux following a change in a climate driver. RF can also be calculated after allowing different types of system response: for example, after allowing stratospheric temperatures to adjust, after allowing both stratospheric and surface temperature to adjust, or after allowing temperatures to adjust everywhere (the equilibrium RF) (Figure 8.1 of Myhre et al. 2013).

In this report, we follow the Intergovernmental Panel on Climate Change (IPCC) recommendation that the RF caused by a forcing agent be evaluated as the net radiative flux change at the tropopause after stratospheric temperatures have adjusted to a new radiative equilibrium while assuming all other variables (for example, temperatures and cloud cover) are held fixed (Box 8.1 of Myhre et al. 2013). A change that results in a net increase in the downward flux (shortwave plus longwave) constitutes a positive RF, normally resulting in a warming of the surface and/or atmosphere and potential changes in other climate parameters. Conversely, a change that yields an increase in the net upward flux constitutes a negative RF, leading to a cooling of the surface and/or atmosphere and potential changes in other climate parameters.

FINAL DRAFT

RF serves as a metric to compare present, past, or future perturbations to the climate system (e.g., Boer and Yu 2003; Gillett et al. 2004; Matthews et al. 2004; Meehl et al. 2004; Jones et al. 2007; Mahajan et al. 2013; Shiogama et al. 2013). For clarity and consistency, RF calculations require that a time period be defined over which the forcing occurs. Here, this period is the industrial era, defined as beginning in 1750 and extending to 2011, unless otherwise noted. The 2011 end date is that adopted by the CMIP5 calculations, which are the basis of RF evaluations by the IPCC (Myhre et al. 2013).

A refinement of the RF concept introduced in the latest IPCC assessment (IPCC 2013) is the use of effective radiative forcing (ERF). ERF for a climate driver is defined as its RF plus rapid adjustment(s) to that RF (Myhre et al. 2013). These rapid adjustments occur on timescales much shorter than, for example, the response of ocean temperatures. For an important subset of climate drivers, ERF is more reliably correlated with the climate response to the forcing than is RF; as such, it is an increasingly used metric when discussing forcing. For atmospheric components, ERF includes rapid adjustments due to direct warming of the troposphere, which produces horizontal temperature variations, variations in the vertical lapse rate, and changes in clouds and vegetation, and it includes the microphysical effects of aerosols on cloud lifetime. Rapid changes in land surface properties (temperature, snow and ice cover, and vegetation) are also included. Not included in ERF are climate responses driven by changes in sea surface temperatures or sea ice cover. For forcing by aerosols in snow (Section 2.3.2), ERF includes the effects of direct warming of the snowpack by particulate absorption (for example, snow-grain size changes). Changes in all of these parameters in response to RF are quantified in terms of their impact on radiative fluxes (for example, albedo) and included in the ERF. The largest differences between RF and ERF occur for forcing by light-absorbing aerosols because of their influence on clouds and snow (Section 2.3.2). For most non-aerosol climate drivers, the differences between RF and ERF are small.

2.3 Drivers of Climate Change over the Industrial Era

Climate drivers of significance over the industrial era include both those associated with anthropogenic activity and, to a lesser extent, those of natural origin. The only significant natural climate drivers in the industrial era are changes in solar irradiance, volcanic eruptions, and the El Niño–Southern Oscillation. Natural emissions and sinks of GHGs and tropospheric aerosols have varied over the industrial era but have not contributed significantly to RF. The effects of cosmic rays on cloud formation have been studied, but global radiative effects are not considered significant (Krissansen-Totton and Davies 2013). There are other known drivers of natural origin that operate on longer timescales (for example, changes in Earth's orbit [Milankovitch cycles] and changes in atmospheric CO_2 via chemical weathering of rock). Anthropogenic drivers can be divided into a number of categories, including well-mixed greenhouse gases (WMGHGs), short-lived climate forcers (SLCFs, which include methane, some hydrofluorocarbons [HFCs], ozone, and aerosols), contrails, and changes in albedo (for example, land-use changes). Some

FINAL DRAFT

WMGHGs are also considered SLCFs (for example, methane). Figures 2.3–2.7 summarize features of the principal climate drivers in the industrial era. Each is described briefly in the following.

[INSERT FIGURE 2.3 HERE]

2.3.1 Natural Drivers

SOLAR IRRADIANCE

Changes in solar irradiance directly impact the climate system because the irradiance is Earth's primary energy source (Lean 1997). In the industrial era, the largest variations in total solar irradiance follow an 11-year cycle (Frölich and Lean 2004; Gray et al. 2010). Direct solar observations have been available since 1978 (Kopp 2014), though proxy indicators of solar cycles are available back to the early 1600s (Kopp et al. 2016). Although these variations amount to only 0.1% of the total solar output of about 1360 W/m^2 (Kopp and Lean 2011), relative variations in irradiance at specific wavelengths can be much larger (tens of percent). Spectral variations in solar irradiance are highest at near-ultraviolet (UV) and shorter wavelengths (Floyd et al. 2003), which are also the most important wavelengths for driving changes in ozone (Ermolli et al. 2013; Bolduc et al. 2015). By affecting ozone concentrations, variations in total and spectral solar irradiance induce discernible changes in atmospheric heating and changes in circulation (Gray et al. 2010; Lockwood 2012; Seppälä et al. 2014). The relationships between changes in irradiance and changes in atmospheric composition, heating, and dynamics are such that changes in total solar irradiance are not directly correlated with the resulting radiative flux changes (Ermolli et al. 2013; Xu and Powell 2013; Gao et al. 2015).

The IPCC estimate of the RF due to changes in total solar irradiance over the industrial era is 0.05 W/m^2 (range: 0.0 to 0.10 W/m^2) (Myhre et al. 2013). This forcing does not account for radiative flux changes resulting from changes in ozone driven by changes in the spectral irradiance. Understanding of the links between changes in spectral irradiance, ozone concentrations, heating rates, and circulation changes has recently improved using, in particular, satellite data starting in 2002 that provide solar spectral irradiance measurements through the UV (Ermolli et al. 2013) along with a series of chemistry–climate modeling studies (Swartz et al. 2012; Chiodo et al. 2014; Dhomse et al. 2013; Ermolli et al. 2013; Bolduc et al. 2015). At the regional scale, circulation changes driven by solar spectral irradiance variations may be significant for some locations and seasons, but are poorly quantified (Lockwood 2012). Despite remaining uncertainties, there is *very high confidence* that solar radiance-induced changes in RF are small relative to RF from anthropogenic GHGs over the industrial era (Myhre et al. 2013) (Figure 2.3).

FINAL DRAFT

VOLCANOES

Most volcanic eruptions are minor events with the effects of emissions confined to the troposphere and only lasting for weeks to months. In contrast, explosive volcanic eruptions inject substantial amounts of sulfur dioxide (SO_2) and ash into the stratosphere, which leads to significant short-term climate effects (Myhre et al. 2013, and references therein). SO_2 oxidizes to form sulfuric acid (H_2SO_4) which condenses, forming new particles or adding mass to preexisting particles, thereby substantially enhancing the attenuation of sunlight transmitted through the stratosphere (that is, increasing aerosol optical depth). These aerosols increase the Earth's albedo by scattering sunlight back to space, creating a negative RF that cools the planet (Andronova et al. 1999; Robock 2000). The RF persists for the lifetime of aerosol in the stratosphere, which is a few years, far exceeding that in the troposphere (about a week). The oceans respond to a negative volcanic RF through cooling and changes in ocean circulation patterns that last for decades after major eruptions (for example, Mt. Tambora in 1815) (Stenchikov et al. 2009; Otterå et al. 2010; Zanchettin et al. 2012; Zhang et al. 2013). In addition to the direct RF, volcanic aerosol heats the stratosphere, altering circulation patterns, and depletes ozone by enhancing surface reactions, which further changes heating and circulation. The resulting impacts on advective heat transport can be larger than the temperature impacts of the direct forcing (Robock 2000). Aerosol from both explosive and non-explosive eruptions also affects the troposphere through changes in diffuse radiation and through aerosol–cloud interactions. It has been proposed that major eruptions might "fertilize" the ocean with sufficient iron to affect phyotoplankton production and, therefore, enhance the ocean carbon sink (Langmann 2014). Volcanoes also emit CO_2 and water vapor, although in small quantities relative to other emissions. At present, conservative estimates of annual CO_2 emissions from volcanoes are less than 1% of CO_2 emissions from all anthropogenic activities (Gerlach 2011). The magnitude of volcanic effects on climate depend on the number and strengths of eruptions, the latitude of injection and, for ocean temperature and circulation impacts, the timing of the eruption relative to ocean temperature and circulation patterns (Zanchettin et al. 2012; Zhang et al. 2013).

Volcanic eruptions represent the largest natural forcing within the industrial era. In the last millennium, eruptions caused several multiyear, transient episodes of negative RF of up to several W/m^2 (Figure 2.6). The RF of the last major volcanic eruption, Mt. Pinatubo in 1991, decayed to negligible values later in the 1990s, with the temperature signal lasting about twice as long due to the effects of changes in ocean heat uptake (Stenchikov et al. 2009). A net volcanic RF has been omitted from the drivers of climate change in the industrial era in Figure 2.3 because the value from multiple, episodic eruptions is negligible compared with the other climate drivers. While future explosive volcanic eruptions have the potential to again alter Earth's climate for periods of several years, predictions of occurrence, intensity, and location remain elusive. If a sufficient number of non-explosive eruptions occur over an extended time period in

FINAL DRAFT

the future, average changes in tropospheric composition or circulation could yield a significant RF (Robock 2000).

2.3.2 Anthropogenic Drivers

PRINCIPAL WELL-MIXED GREENHOUSE GASES (WMGHGs)

The principal WMGHGs are carbon dioxide (CO_2), methane (CH_4), and nitrous oxide (N_2O). With atmospheric lifetimes of a decade or more, these gases have modest-to-small regional variabilities and are circulated and mixed around the globe to yield small interhemispheric gradients. The atmospheric abundances and associated radiative forcings of WMGHGs have increased substantially over the industrial era (Figures 2.4–2.6). Contributions from natural sources of these constituents are accounted for in the industrial-era RF calculations shown in Figure 2.6.

[INSERT FIGURES 2.4, 2.5, AND 2.6 HERE]

CO_2 has substantial global sources and sinks (Figure 2.7). CO_2 emission sources have grown in the industrial era primarily from fossil fuel combustion (that is, coal, gas, and oil), cement manufacturing, and land-use change from activities such as deforestation (Ciais et al. 2013). Carbonation of finished cement products is a sink of atmospheric CO_2, offsetting a substantial fraction (0.43) of the industrial-era emissions from cement production (Xi et al. 2016). A number of processes act to remove CO_2 from the atmosphere, including uptake in the oceans, residual land uptake, and rock weathering. These combined processes yield an effective atmospheric lifetime for emitted CO_2 of many decades to millennia, far greater than any other major GHG. Seasonal variations in CO_2 atmospheric concentrations occur in response to seasonal changes in photosynthesis in the biosphere, and to a lesser degree to seasonal variations in anthropogenic emissions. In addition to fossil fuel reserves, there are large natural reservoirs of carbon in the oceans, in vegetation and soils, and in permafrost.

In the industrial era, the CO_2 atmospheric growth rate has been exponential (Figure 2.4), with the increase in atmospheric CO_2 approximately twice that absorbed by the oceans. Over at least the last 50 years, CO_2 has shown the largest annual RF increases among all GHGs (Figures 2.4 and 2.5). The global average CO_2 concentration has increased by 40% over the industrial era, increasing from 278 parts per million (ppm) in 1750 to 390 ppm in 2011 (Ciais et al. 2013); it now exceeds 400 ppm (as of 2016) (http://www.esrl.noaa.gov/gmd/ccgg/trends/). CO_2 has been chosen as the reference in defining the global warming potential (GWP) of other GHGs and climate agents. The GWP of a GHG is the integrated RF over a specified time period (for example, 100 years) from the emission of a given mass of the GHG divided by the integrated RF from the same mass emission of CO_2.

[INSERT FIGURE 2.7 HERE]

FINAL DRAFT

The global mean methane concentration and RF have also grown substantially in the industrial era (Figures 2.4 and 2.5). Methane is a stronger GHG than CO_2 for the same emission mass and has a shorter atmospheric lifetime of about 12 years. Methane also has indirect climate effects through induced changes in CO_2, stratospheric water vapor, and ozone (Lelieveld and Crutzen 1992). The 100-year GWP of methane is 28–36, depending on whether oxidation into CO_2 is included and whether climate-carbon feedbacks are accounted for; its 20-year GWP is even higher (84–86) (Myhre et al. 2013 Table 8.7). With a current global mean value near 1840 parts per billion by volume (ppb), the methane concentration has increased by a factor of about 2.5 over the industrial era. The annual growth rate for methane has been more variable than that for CO_2 and N_2O over the past several decades, and has occasionally been negative for short periods.

Methane emissions, which have a variety of natural and anthropogenic sources, totaled 556 ± 56 Tg CH_4 in 2011 based on top-down analyses, with about 60% from anthropogenic sources (Ciais et al. 2013). The methane budget is complicated by the variety of natural and anthropogenic sources and sinks that influence its atmospheric concentration. These include the global abundance of the hydroxyl radical (OH), which controls the methane atmospheric lifetime; changes in large-scale anthropogenic activities such as mining, natural gas extraction, animal husbandry, and agricultural practices; and natural wetland emissions (Table 6.8, Ciais et al. 2013). The remaining uncertainty in the cause(s) of the approximately 20-year negative trend in the methane annual growth rate starting in the mid-1980s and the rapid increases in the annual rate in the last decade (Figure 2.4) reflect the complexity of the methane budget (Ciais et al. 2013; Saunois et al. 2016; Nisbet et al. 2016).

Growth rates in the global mean nitrous oxide (N_2O) concentration and RF over the industrial era are smaller than for CO_2 and methane (Figures 2.4 and 2.5). N_2O is emitted in the nitrogen cycle in natural ecosystems and has a variety of anthropogenic sources, including the use of synthetic fertilizers in agriculture, motor vehicle exhaust, and some manufacturing processes. The current global value near 330 ppb reflects steady growth over the industrial era with average increases in recent decades of 0.75 ppb per year (Ciais et al. 2013) (Figure 2.4). Fertilization in global food production is responsible for about 80% of the growth rate. Anthropogenic sources account for approximately 40% of the annual N_2O emissions of 17.9 (8.1 to 30.7) TgN (Ciais et al., 2013). N_2O has an atmospheric lifetime of about 120 years and a GWP in the range 265–298 (Myhre et al. 2013 Table 8.7). The primary sink of N_2O is photochemical destruction in the stratosphere, which produces nitrogen oxides (NO_x) that catalytically destroy ozone (e.g., Skiba and Rees 2014). Small indirect climate effects, such as the response of stratospheric ozone, are generally not included in the N_2O RF.

N_2O is a component of the larger global budget of total nitrogen (N) comprising N_2O, ammonia (NH_3), and reactive nitrogen (NO_x). Significant uncertainties are associated with balancing this budget over oceans and land while accounting for deposition and emission processes (Ciais et al. 2013; Fowler et al. 2013). Furthermore, changes in climate parameters such as temperature,

FINAL DRAFT

moisture, and CO_2 concentrations are expected to affect the N_2O budget in the future, and perhaps atmospheric concentrations.

OTHER WELL-MIXED GREENHOUSE GASES

Other WMGHGs include several categories of synthetic (i.e., manufactured) gases, including chlorofluorocarbons (CFCs), halons, hydrochlorofluorocarbons (HCFCs), hydrofluorocarbons (HFCs), perfluorocarbons (PFCs), and sulfur hexafluoride (SF_6), collectively known as halocarbons. Natural sources of these gases in the industrial era are small compared to anthropogenic sources. Important examples are the expanded use of CFCs as refrigerants and in other applications beginning in the mid-20th century. The atmospheric abundances of principal CFCs began declining in the 1990s after their regulation under the Montreal Protocol as substances that deplete stratospheric ozone (Figure 2.4). All of these gases are GHGs covering a wide range of GWPs, atmospheric concentrations, and trends. PFCs, SF_6, and HFCs are in the basket of gases covered under the United Nations Framework Convention on Climate Change. The United States joined other countries in proposing that HFCs be controlled as a WMGHGs under the Montreal Protocol because of their large projected future abundances (Velders et al. 2015). In October 2016, the Montreal Protocol adopted an amendment to phase down global HFC production and consumption, avoiding emissions equivalent to approximately 105 Gt CO_2 by 2100 based on earlier projections (Velders et al. 2015). The atmospheric growth rates of some halocarbon concentrations are significant at present (for example, SF_6 and HFC-134a), although their RF contributions remain small (Figure 2.5).

WATER VAPOR

Water vapor in the atmosphere acts as a powerful natural GHG, significantly increasing the Earth's equilibrium temperature. In the stratosphere, water vapor abundances are controlled by transport from the troposphere and from oxidation of methane. Increases in methane from anthropogenic activities therefore increase stratospheric water vapor, producing a positive RF (e.g., Solomon et al. 2010; Hegglin et al. 2014). Other less-important anthropogenic sources of stratospheric water vapor are hydrogen oxidation (le Texier et al. 1988), aircraft exhaust (Rosenlof et al. 2001; Morris et al. 2003), and explosive volcanic eruptions (Löffler et al. 2016).

In the troposphere, the amount of water vapor is controlled by temperature (Held and Soden 2000). Atmospheric circulation, especially convection, limits the buildup of water vapor in the atmosphere such that the water vapor from direct emissions, for example by combustion of fossil fuels or by large power plant cooling towers, does not accumulate in the atmosphere but actually offsets water vapor that would otherwise evaporate from the surface. Direct changes in atmospheric water vapor are negligible in comparison to the indirect changes caused by temperature changes resulting from radiative forcing. As such, changes in tropospheric water vapor are considered a feedback in the climate system (see Section 2.6.1 and Figure 2.2). As

FINAL DRAFT

increasing GHG concentrations warm the atmosphere, tropospheric water vapor concentrations increase, thereby amplifying the warming effect (Held and Soden 2000).

OZONE

Ozone is a naturally occurring GHG in the troposphere and stratosphere and is produced and destroyed in response to a variety of anthropogenic and natural emissions. Ozone abundances have high spatial and temporal variability due to the nature and variety of the production, loss, and transport processes controlling ozone abundances, which adds complexity to the ozone RF calculations. In the global troposphere, emissions of methane, NO_x, carbon monoxide (CO), and non-methane volatile organic compounds (VOCs) form ozone photochemically both near and far downwind of these precursor source emissions, leading to regional and global positive RF contributions (e.g., Dentener et al. 2005). Stratospheric ozone is destroyed photochemically in reactions involving the halogen species chlorine and bromine. Halogens are released in the stratosphere from the decomposition of some halocarbons emitted at the surface (WMO 2014). Stratospheric ozone depletion, which is most notable in the polar regions, yields a net negative RF (Myhre et al. 2013).

AEROSOLS

Atmospheric aerosols are perhaps the most complex and most uncertain component of forcing due to anthropogenic activities (Myhre et al. 2013). Aerosols have diverse natural and anthropogenic sources, and emissions from these sources interact in non-linear ways (Boucher et al. 2013). Aerosol types are categorized by composition; namely, sulfate, black carbon, organic, nitrate, dust, and sea salt. Individual particles generally include a mix of these components due to chemical and physical transformations of aerosols and aerosol precursor gases following emission. Aerosol tropospheric lifetimes are days to weeks due to the general hygroscopic nature of primary and secondary particles and the ubiquity of cloud and precipitation systems in the troposphere. Particles that act as cloud condensation nuclei (CCN) or are scavenged by cloud droplets are removed from the troposphere in precipitation. The heterogeneity of aerosol sources and locations combined with short aerosol lifetimes leads to the high spatial and temporal variabilities observed in the global aerosol distribution and their associated forcings.

Aerosols from anthropogenic activities influence RF in three primary ways: through aerosol–radiation interactions, through aerosol–cloud interactions, and through albedo changes from absorbing-aerosol deposition on snow and ice (Boucher et al. 2013). RF from aerosol–radiation interactions, also known as the aerosol "direct effect," involves absorption and scattering of longwave and shortwave radiation. RF from aerosol-cloud interactions, also known as the cloud albedo "indirect effect," results from changes in cloud droplet number and size due to changes in aerosol (cloud condensation nuclei) number and composition. The RF for the global net aerosol–radiation and aerosol–cloud interaction is negative (Myhre et al. 2013). However, the RF is not negative for all aerosol types. Light-absorbing aerosols, such as black carbon, absorb sunlight,

FINAL DRAFT

producing a positive RF. This absorption warms the atmosphere; on net, this response is assessed to increase cloud cover and therefore increase planetary albedo (the "semi-direct" effect). This "rapid response" lowers the ERF of atmospheric black carbon by approximately 15% relative to its RF from direct absorption alone (Bond et al. 2013). ERF for aerosol–cloud interactions includes this rapid adjustment for absorbing aerosol (that is, the cloud response to atmospheric heating) and it includes cloud lifetime effects (for example, glaciation and thermodynamic effects) (Boucher et al. 2013). Light-absorbing aerosols also affect climate when present in surface snow by lowering surface albedo, yielding a positive RF (e.g. Flanner et al. 2009). For black carbon deposited on snow, the ERF is a factor of three higher than the RF because of positive feedbacks that reduce snow albedo and accelerate snow melt (e.g., Flanner et al. 2009; Bond et al. 2013). There is *very high confidence* that the RF from snow and ice albedo is positive (Bond et al. 2013).

LAND SURFACE

Land-cover changes (LCC) due to anthropogenic activities in the industrial era have changed the land surface brightness (albedo), principally through deforestation and afforestation. There is strong evidence that these changes have increased Earth's global surface albedo, creating a negative (cooling) RF of -0.15 ± 0.10 W/m^2 (Myhre et al. 2013). In specific regions, however, LCC has lowered surface albedo producing a positive RF (for example, through afforestation and pasture abandonment). In addition to the direct radiative forcing through albedo changes, LCC also have indirect forcing effects on climate, such as altering carbon cycles and altering dust emissions through effects on the hydrologic cycle. These effects are generally not included in the direct LCC RF calculations and are instead included in the net GHG and aerosol RFs over the industrial era. These indirect forcings may be of opposite sign to that of the direct LCC albedo forcing and may constitute a significant fraction of industrial-era RF driven by human activities (Ward et al. 2014). Some of these effects, such as alteration of the carbon cycle, constitute climate feedbacks (Figure 2.2) and are discussed more extensively in Chapter 10: Land Cover. The increased use of satellite observations to quantify LCC has resulted in smaller negative LCC RF values (e.g., Ju and Masek 2016). In areas with significant irrigation, surface temperatures and precipitation are affected by a change in energy partitioning from sensible to latent heating. Direct RF due to irrigation is generally small and can be positive or negative, depending on the balance of longwave (surface cooling or increases in water vapor) and shortwave (increased cloudiness) effects (Cook et al. 2015).

CONTRAILS

Line-shaped (linear) contrails are a special type of cirrus cloud that forms in the wake of jet-engine aircraft operating in the mid- to upper troposphere under conditions of high ambient humidity. Persistent contrails, which can last for many hours, form when ambient humidity conditions are supersaturated with respect to ice. As persistent contrails spread and drift with the local winds after formation, they lose their linear features, creating additional cirrus cloudiness

FINAL DRAFT

that is indistinguishable from background cloudiness. Contrails and contrail cirrus are additional forms of cirrus cloudiness that interact with solar and thermal radiation to provide a global net positive RF and thus are visible evidence of an anthropogenic contribution to climate change (Burkhardt and Kärcher 2011).

2.4 Industrial-era Changes in Radiative Forcing Agents

The IPCC best-estimate values of present day RFs and ERFs from principal anthropogenic and natural climate drivers are shown in Figure 2.3 and in Table 2.1. The past changes in the industrial era leading up to present day RF are shown for anthropogenic gases in Figure 2.5 and for all climate drivers in Figure 2.6.

The combined figures have several striking features. First, there is a large range in the magnitudes of RF terms, with contrails, stratospheric ozone, black carbon on snow, and stratospheric water vapor being small fractions of the largest term (CO_2). The sum of ERFs from CO_2 and non-CO_2 GHGs, tropospheric ozone, stratospheric water, contrails, and black carbon on snow shows a gradual increase from 1750 to the mid-1960s and accelerated annual growth in the subsequent 50 years (Figure 2.6). The sum of aerosol effects, stratospheric ozone depletion, and land use show a monotonically increasing cooling trend for the first two centuries of the depicted time series. During the past several decades, however, this combined cooling trend has leveled off due to reductions in the emissions of aerosols and aerosol precursors, largely as a result of legislation designed to improve air quality (Smith and Bond 2014; Fiore et al. 2015). In contrast, the volcanic RF reveals its episodic, short-lived characteristics along with large values that at times dominate the total RF. Changes in total solar irradiance over the industrial era are dominated by the 11-year solar cycle and other short-term variations. The solar irradiance RF between 1745 and 2005 is 0.05 (range of 0.0–0.1) W/m^2 (Myhre et al. 2013), a very small fraction of total anthropogenic forcing in 2011. The large relative uncertainty derives from inconsistencies among solar models, which all rely on proxies of solar irradiance to fit the industrial era. In total, ERF has increased substantially in the industrial era, driven almost completely by anthropogenic activities, with annual growth in ERF notably higher after the mid-1960s.

The principal anthropogenic activities that have increased ERF are those that increase net GHG emissions. The atmospheric concentrations of CO_2, CH_4, and N_2O are higher now than they have been in at least the past 800,000 years (Masson-Delmotte et al. 2013). All have increased monotonically over the industrial era (Figure 2.4), and are now 40%, 250%, and 20%, respectively, above their preindustrial concentrations as reflected in the RF time series in Figure 2.5. Tropospheric ozone has increased in response to growth in precursor emissions in the industrial era. Emissions of synthetic GHGs have grown rapidly beginning in the mid-20th century, with many bringing halogens to the stratosphere and causing ozone depletion in subsequent decades. Aerosol RF effects are a sum over aerosol–radiation and aerosol–cloud interactions; this RF has increased in the industrial era due to increased emissions of aerosol and

FINAL DRAFT

aerosol precursors (Figure 2.6). These global aerosol RF trends average across disparate trends at the regional scale. The recent leveling off of global aerosol concentrations is the result of declines in many regions that were driven by enhanced air quality regulations, particularly starting in the 1980s (e.g., Philipona et al. 2009; Liebensperger et al. 2012; Wild 2016). These declines are partially offset by increasing trends in other regions, such as much of Asia and possibly the Arabian Peninsula (Hsu et al. 2012; Chin et al. 2014; Lynch et al. 2016). In highly polluted regions, negative aerosol RF may fully offset positive GHG RF, in contrast to global annual averages in which positive GHG forcing fully offsets negative aerosol forcing (Figures 2.3 and 2.6).

2.5 The Complex Relationship between Concentrations, Forcing, and Climate Response

Climate changes occur in response to ERFs, which generally include certain rapid responses to the underlying RF terms. (Figure 2.2). Responses within the Earth system to forcing can act to either amplify (positive feedback) or reduce (negative feedback) the original forcing. These feedbacks operate on a range of timescales, from days to centuries. Thus, in general, the full climate impact of a given forcing is not immediately realized. Of interest are the climate response at a given point in time under continuously evolving forcings and the total climate response realized for a given forcing. A metric for the former, which approximates near-term climate change from a GHG forcing, is the transient climate response (TCR), defined as the change in global mean surface temperature when the atmospheric CO_2 concentration has doubled in a scenario of concentration increasing at 1% per year. The latter is given by the equilibrium climate sensitivity (ECS), defined as the change at equilibrium in annual and global mean surface temperature following a doubling of the atmospheric CO_2 concentration (Flato et al. 2013). TCR is more representative of near-term climate change from a GHG forcing. To estimate ECS, climate model runs have to simulate thousands of years in order to allow sufficient time for ocean temperatures to reach equilibrium.

In the IPCC's Fifth Assessment Report, ECS is assessed to be a factor of 1.5 or more greater than the TCR (ECS is 2.7°F to 8.1°F [1.5°C to 4.5°C] and TCR is 1.8°F to 4.5°F [1.0°C to 2.5°C]; Flato et al. 2013), exemplifying that longer time-scale feedbacks are both significant and positive. Confidence in the model-based TCR and ECS values is increased by their agreement, within respective uncertainties, with other methods of calculating these metrics (Collins et al. 2013; Box 12.2). The alternative methods include using reconstructed temperatures from paleoclimate archives, the forcing/response relationship from past volcanic eruptions, and observed surface and ocean temperature changes over the industrial era (Collins et al. 2013).

While TCR and ECS are defined specifically for the case of doubled CO_2, the climate sensitivity factor, λ, more generally relates the equilibrium surface temperature response (ΔT) to a constant forcing (ERF) as given by $\Delta T = \lambda ERF$ (Knutti and Hegerl 2008; Flato et al. 2013). The λ factor

FINAL DRAFT

is highly dependent on feedbacks within the Earth system; all feedbacks are quantified themselves as radiative forcings, since each one acts by affecting Earth's albedo or its greenhouse effect. Models in which feedback processes are more positive (that is, more strongly amplify warming) tend to have a higher climate sensitivity (see Figure 9.43 of Flato et al. 2013). In the absence of feedbacks, λ would be equal to 0.54°F/(W/m^2) (0.30°C/[W/m^2]). The magnitude of λ for ERF over the industrial era varies across models, but in all cases λ is greater than 0.54°F/(W/m^2), indicating the sum of all climate feedbacks tends to be positive. Overall, the global warming response to ERF includes a substantial amplification from feedbacks, with a model mean λ of 0.86°F/(W/m^2) (0.48°C/[W/m^2]) with a 90% uncertainty range of ±0.23°F/(W/m^2) (±0.13°C/[W/m^2]) (as derived from climate sensitivity parameter in Table 9.5 of Flato et al. [2013] combined with methodology of Bony et al. [2006]). Thus, there is *high confidence* that the response of the Earth system to the industrial-era net positive forcing is to amplify that forcing (Figure 9.42 of Flato et al. 2013).

The models used to quantify λ account for the near-term feedbacks described below (Section 2.6.1), though with mixed levels of detail regarding feedbacks to atmospheric composition. Feedbacks to the land and ocean carbon sink, land albedo and ocean heat uptake, most of which operate on longer timescales (Section 2.6.2), are currently included on only a limited basis, or in some cases not at all, in climate models. Climate feedbacks are the largest source of uncertainty in quantifying climate sensitivity (Flato et al. 2013); namely, the responses of clouds, the carbon cycle, ocean circulation and, to a lesser extent, land and sea ice to surface temperature and precipitation changes.

The complexity of mapping forcings to climate responses on a global scale is enhanced by geographic and seasonal variations in these forcings and responses, driven in part by similar variations in anthropogenic emissions and concentrations. Studies show that the spatial pattern and timing of climate responses are not always well correlated with the spatial pattern and timing of a radiative forcing, since adjustments within the climate system can determine much of the response (e.g., Shindell and Faluvegi 2009; Crook and Forster 2011; Knutti and Rugenstein 2015). The RF patterns of short-lived climate drivers with inhomogeneous source distributions, such as aerosols, tropospheric ozone, contrails, and land cover change, are leading examples of highly inhomogeneous forcings. Spatial and temporal variability in aerosol and aerosol precursor emissions is enhanced by in-atmosphere aerosol formation and chemical transformations, and by aerosol removal in precipitation and surface deposition. Even for relatively uniformly distributed species (for example, WMGHGs), RF patterns are less homogenous than their concentrations. The RF of a uniform CO_2 distribution, for example, depends on latitude and cloud cover (Ramanathan et al. 1979). With the added complexity and variability of regional forcings, the global mean RFs are known with more confidence than the regional RF patterns. Forcing feedbacks in response to spatially variable forcings also have variable geographic and temporal patterns.

FINAL DRAFT

Quantifying the relationship between spatial RF patterns and regional and global climate responses in the industrial era is difficult because it requires distinguishing forcing responses from the inherent internal variability of the climate system, which acts on a range of time scales. The ability to test the accuracy of modeled responses to forcing patterns is limited by the sparsity of long-term observational records of regional climate variables. As a result, there is generally *very low confidence* in our understanding of the qualitative and quantitative forcing–response relationships at the regional scale. However, there is *medium to high confidence* in other features, such as aerosol effects altering the location of the Inter Tropical Convergence Zone (ITCZ) and the positive feedback to reductions of snow and ice and albedo changes at high latitudes (Boucher et al. 2013; Myhre et al. 2013).

2.6 Radiative-forcing Feedbacks

2.6.1 Near-term Feedbacks

PLANCK FEEDBACK

When the temperatures of Earth's surface and atmosphere increase in response to RF, more infrared radiation is emitted into the lower atmosphere; this serves to restore radiative balance at the tropopause. This radiative feedback, defined as the Planck feedback, only partially offsets the positive RF while triggering other feedbacks that affect radiative balance. The Planck feedback magnitude is -3.20 ± 0.04 W/m^2 per 1.8°F (1°C) of warming and is the strongest and primary stabilizing feedback in the climate system (Vial et al. 2013).

WATER VAPOR AND LAPSE RATE FEEDBACKS

Warmer air holds more moisture (water vapor) than cooler air—about 7% more per degree Celsius—as dictated by the Clausius–Clapeyron relationship (Allen and Igram 2002). Thus, as global temperatures increase, the total amount of water vapor in the atmosphere increases, adding further to greenhouse warming—a positive feedback—with a mean value derived from a suite of atmosphere/ocean global climate models (AOGCM) of 1.6 ± 0.3 W/m^2 per 1.8°F (1°C) of warming (Flato et al. 2013, Table 9.5). The water vapor feedback is responsible for more than doubling the direct climate warming from CO_2 emissions alone (Bony et al. 2006; Soden and Held 2006; Vial et al. 2013). Observations confirm that global tropospheric water vapor has increased commensurate with measured warming (IPCC 2013, FAQ 3.2 and Figure 1a). Interannual variations and trends in stratospheric water vapor, while influenced by tropospheric abundances, are controlled largely by tropopause temperatures and dynamical processes (Dessler et al. 2014). Increases in tropospheric water vapor have a larger warming effect in the upper troposphere (where it is cooler) than in the lower troposphere, thereby decreasing the rate at which temperatures decrease with altitude (the lapse rate). Warmer temperatures aloft increase outgoing infrared radiation—a negative feedback—with a mean value derived from the same AOGCM suite of -0.6 ± 0.4 W/m^2 per 1.8°F (1°C) warming. These feedback values remain

FINAL DRAFT

largely unchanged between recent IPCC assessments (IPCC 2007; 2013). Recent advances in both observations and models have increased confidence that the net effect of the water vapor and lapse rate feedbacks is a significant positive RF (Flato et al. 2013).

CLOUD FEEDBACKS

An increase in cloudiness has two direct impacts on radiative fluxes: first, it increases scattering of sunlight, which increases Earth's albedo and cools the surface (the shortwave cloud radiative effect); second, it increases trapping of infrared radiation, which warms the surface (the longwave cloud radiative effect). A decrease in cloudiness has the opposite effects. Clouds have a relatively larger shortwave effect when they form over dark surfaces (for example, oceans) than over higher albedo surfaces, such as sea ice and deserts. For clouds globally, the shortwave cloud radiative effect is about –50 W/m^2 and the longwave effect is about +30 W/m^2, yielding a net cooling influence (Loeb et al. 2009; Sohn et al. 2010). The relative magnitudes of both effects vary with cloud type as well as with location. For low-altitude, thick clouds (for example, stratus and stratocumulus) the shortwave radiative effect dominates, so they cause a net cooling. For high-altitude, thin clouds (for example, cirrus) the longwave effect dominates, so they cause a net warming (e.g., Hartmann et al. 1992; Chen et al. 2000). Therefore, an increase in low clouds is a negative feedback to RF, while an increase in high clouds is a positive feedback. The potential magnitude of cloud feedbacks is large compared with global RF (see Section 2.4). Cloud feedbacks also influence natural variability within the climate system and may amplify atmospheric circulation patterns and the El Niño–Southern Oscillation (Rädel et al. 2016).

The net radiative effect of cloud feedbacks is positive over the industrial era, with an assessed value of +0.27 ± 0.42 W/m^2 per 1.8°F (1°C) warming (Vial et al. 2013). The net cloud feedback can be broken into components, where the longwave cloud feedback is positive (+0.24 ± 0.26 W/m^2 per 1.8°F [1°C] warming) and the shortwave feedback is near-zero (+0.14 ± 0.40 W/m^2 per 1.8°F [1°C] warming; Vial et al. 2013), though the two do not add linearly. The value of the shortwave cloud feedback shows a significant sensitivity to computation methodology (Taylor et al. 2011; Vial et al. 2013; Klocke et al. 2013). Uncertainty in cloud feedback remains the largest source of inter-model differences in calculated climate sensitivity (Vial et al. 2013; Boucher et al. 2013).

SNOW, ICE, AND SURFACE ALBEDO

Snow and ice are highly reflective to solar radiation relative to land surfaces and the ocean. Loss of snow cover, glaciers, ice sheets, or sea ice resulting from climate warming lowers Earth's surface albedo. The losses create the snow-albedo feedback because subsequent increases in absorbed solar radiation lead to further warming as well as changes in turbulent heat fluxes at the surface (Sejas et al. 2014). For seasonal snow, glaciers, and sea ice, a positive albedo feedback occurs where light-absorbing aerosols are deposited to the surface, darkening the snow and ice

FINAL DRAFT

and accelerating the loss of snow and ice mass (e.g., Hansen and Nazarenko 2004; Jacobson 2004; Flanner et al. 2009; Skeie et al. 2011; Bond et al. 2013; Yang et al. 2015).

For ice sheets (for example, on Antarctica and Greenland—see Ch. 11: Arctic Changes), the positive radiative feedback is further amplified by dynamical feedbacks on ice-sheet mass loss. Specifically, since continental ice shelves limit the discharge rates of ice sheets into the ocean; any melting of the ice shelves accelerates the discharge rate, creating a positive feedback on the ice-stream flow rate and total mass loss (e.g., Holland et al. 2008; Schoof 2010; Rignot et al. 2010; Joughin et al. 2012). Warming oceans also lead to accelerated melting of basal ice (ice at the base of a glacier or ice sheet) and subsequent ice-sheet loss (e.g., Straneo et al. 2013; Thoma et al. 2015; Alley et al. 2016; Silvano et al. 2016). Feedbacks related to ice sheet dynamics occur on longer timescales than other feedbacks—many centuries or longer. Significant ice-sheet melt can also lead to changes in freshwater input to the oceans, which in turn can affect ocean temperatures and circulation, ocean–atmosphere heat exchange and moisture fluxes, and atmospheric circulation (Masson-Delmotte et al. 2013).

The complete contribution of ice-sheet feedbacks on timescales of millennia are not generally included in CMIP5 climate simulations. These slow feedbacks are also not thought to change in proportion to global mean surface temperature change, implying that the apparent climate sensitivity changes with time, making it difficult to fully understand climate sensitivity considering only the industrial age. This slow response increases the likelihood for tipping points, as discussed further in Chapter 15: Potential Surprises.

The surface-albedo feedback is an important influence on interannual variations in sea ice as well as on long-term climate change. While there is a significant range in estimates of the snow-albedo feedback, it is assessed as positive (Hall and Qu 2006; Fernandes et al. 2009; Vial et al. 2013), with a best estimate of 0.27 ± 0.06 W/m^2 per 1.8°F (1°C) of warming globally. Within the cryosphere, the surface-albedo feedback is most effective in polar regions (Winton 2006; Taylor et al. 2011); there is also evidence that polar surface-albedo feedbacks might influence the tropical climate as well (Hall 2004).

Changes in sea ice can also influence Arctic cloudiness. Recent work indicates that Arctic clouds have responded to sea ice loss in fall but not summer (Kay and Gettelman 2009; Kay et al. 2011; Kay and L'Ecuyer 2013; Pistone et al. 2014; Taylor et al. 2015). This has important implications for future climate change, as an increase in summer clouds could offset a portion of the amplifying surface-albedo feedback, slowing down the rate of arctic warming.

ATMOSPHERIC COMPOSITION

Climate change alters the atmospheric abundance and distribution of some radiatively active species by changing natural emissions, atmospheric photochemical reaction rates, atmospheric lifetimes, transport patterns, or deposition rates. These changes in turn alter the associated ERFs, forming a feedback (Liao et al. 2009; Unger et al. 2009; Raes et al. 2010). Atmospheric

FINAL DRAFT

composition feedbacks occur through a variety of processes. Important examples include climate-driven changes in temperature and precipitation that affect 1) natural sources of NO_x from soils and lightning and VOC sources from vegetation, all of which affect ozone abundances (Raes et al. 2010; Tai et al. 2013; Yue et al. 2015); 2) regional aridity, which influences surface dust sources as well as susceptibility to wildfires; and 3) surface winds, which control the emission of dust from the land surface and the emissions of sea salt and dimethyl sulfide—a natural precursor to sulfate aerosol—from the ocean surface.

Climate-driven ecosystem changes that alter the carbon cycle potentially impact atmospheric CO_2 and CH_4 abundances (Section 2.6.2). Atmospheric aerosols affect clouds and precipitation rates, which in turn alter aerosol removal rates, lifetimes, and atmospheric abundances. Longwave radiative feedbacks and climate-driven circulation changes also alter stratospheric ozone abundance (Nowack et al. 2015). Investigation of these and other composition–climate interactions is an active area of research (e.g., John et al. 2012; Pacifico et al. 2012; Morgenstern et al. 2013; Holmes et al. 2013; Naik et al. 2013; Voulgarakis et al. 2013; Isaksen et al. 2014; Dietmuller et al. 2014; Banerjee et al. 2014). While understanding of key processes is improving, atmospheric composition feedbacks are absent or limited in many global climate modeling studies used to project future climate, though this is rapidly changing (ACC-MIP 2017). For some composition–climate feedbacks involving shorter-lived constituents, the net effects may be near-zero at the global scale while significant at local to regional scales (e.g. Raes et al. 2010; Han et al. 2013).

2.6.2 Long-term Feedbacks

TERRESTRIAL ECOSYSTEMS AND CLIMATE CHANGE FEEDBACKS

The cycling of carbon through the climate system is an important long-term climate feedback that affects atmospheric CO_2 concentrations. The global mean atmospheric CO_2 concentration is determined by emissions from burning fossil fuels, wildfires, and permafrost thaw balanced against CO_2 uptake by the oceans and terrestrial biosphere (Ciais et al. 2013; Le Quéré et al. 2016) (Figures 2.2 and 2.7). During the past decade, just less than a third of anthropogenic CO_2 has been taken up by the terrestrial environment, and another quarter by the oceans (Le Quéré et al. 2016 Table 8) through photosynthesis and through direct absorption by ocean surface waters. The capacity of the land to continue uptake of CO_2 is uncertain and depends on land-use management and on responses of the biosphere to climate change (see Ch. 10: Land Cover). Altered uptake rates affect atmospheric CO_2 abundance, forcing, and rates of climate change. Such changes are expected to evolve on the decadal and longer timescale, though abrupt changes are possible.

Significant uncertainty exists in quantification of carbon-cycle feedbacks. Differences in the assumed characteristics of the land carbon-cycle processes are the primary cause of the inter-model spread in modeling the present-day carbon cycle and a leading source of uncertainty.

FINAL DRAFT

Significant uncertainties also exist in ocean carbon-cycle changes in future climate scenarios. Basic principles of carbon cycle dynamics in terrestrial ecosystems suggest that increased atmospheric CO_2 concentrations can directly enhance plant growth rates and, therefore, increase carbon uptake (the "CO_2 fertilization" effect), nominally sequestering much of the added carbon from fossil-fuel combustion (e.g., Wenzel et al. 2016). However, this effect is variable; sometimes plants acclimate so that higher CO_2 concentrations no longer enhance growth (e.g., Franks et al. 2013). In addition, CO_2 fertilization is often offset by other factors limiting plant growth, such as water and or nutrient availability and temperature and incoming solar radiation that can be modified by changes in vegetation structure. Large-scale plant mortality through fire, soil moisture drought, and/or temperature changes also impact successional processes that contribute to reestablishment and revegetation (or not) of disturbed ecosystems, altering the amount and distribution of plants available to uptake CO_2. With sufficient disturbance, it has been argued that forests could, on net, turn into a source rather than a sink of CO_2 (Seppälä 2009).

Climate-induced changes in the horizontal (for example, landscape to biome) and vertical (soils to canopy) structure of terrestrial ecosystems also alter the physical surface roughness and albedo, as well as biogeochemical (carbon and nitrogen) cycles and biophysical evapotranspiration and water demand. Combined, these responses constitute climate feedbacks by altering surface albedo and atmospheric GHG abundances. Drivers of these changes in terrestrial ecosystems include changes in the biophysical growing season, altered seasonality, wildfire patterns, and multiple additional interacting factors (Ch.10: Land Cover).

Accurate determination of future CO_2 stabilization scenarios depends on accounting for the significant role that the land biosphere plays in the global carbon cycle and feedbacks between climate change and the terrestrial carbon cycle (Hibbard et al. 2007). Earth System Models (ESMs) are increasing the representation of terrestrial carbon cycle processes, including plant photosynthesis, plant and soil respiration and decomposition, and CO_2 fertilization, with the latter based on the assumption that an increased atmospheric CO_2 concentration provides more substrate for photosynthesis and productivity. Recent advances in ESMs are beginning to account for other important factors such as nutrient limitations (Thornton et al. 2007; Brzostek et al. 2014; Wieder et al. 2015). ESMs that do include carbon-cycle feedbacks appear, on average, to overestimate terrestrial CO_2 uptake under the present-day climate (Anav et al. 2013; Smith et al. 2016) and underestimate nutrient limitations to CO_2 fertilization (Wieder et al. 2015). The sign of the land carbon-cycle feedback through 2100 remains unclear in the newest generation of ESMs (Friedlingstein et al. 2006, 2014; Wieder et al. 2015). Eleven CMIP5 ESMs forced with the same CO_2 emissions scenario—one consistent with RCP8.5 concentrations—produce a range of 795 to 1145 ppm for atmospheric CO_2 concentration in 2100. The majority of the ESMs (7 out of 11) simulated a CO_2 concentration larger (by 44 ppm on average) than their equivalent non-interactive carbon cycle counterpart (Friedlingstein et al. 2014). This difference in CO_2 equates to about 0.4°F (0.2°C) more warming by 2100. The inclusion of carbon-cycle feedbacks does not

FINAL DRAFT

alter the lower-end bound on climate sensitivity, but, in most climate models, inclusion pushes the upper bound higher (Friedlingstein et al. 2014).

OCEAN CHEMISTRY, ECOSYSTEM, AND CIRCULATION CHANGES

The ocean plays a significant role in climate change by playing a critical role in controlling the amount of GHGs (including CO_2, water vapor, and N_2O) and heat in the atmosphere (Figure 2.7). To date most of the net energy increase in the climate system from anthropogenic RF is in the form of ocean heat (Rhein et al. 2013; see Box 3.1 Figure 1). This additional heat is stored predominantly (about 60%) in the upper 700 meters of the ocean (Johnson et al. 2016 and see Ch. 12: Sea Level Rise and Ch. 13: Ocean Changes). Ocean warming and climate-driven changes in ocean stratification and circulation alter oceanic biological productivity and therefore CO_2 uptake; combined, these feedbacks affect the rate of warming from radiative forcing.

Marine ecosystems take up CO_2 from the atmosphere in the same way that plants do on land. About half of the global net primary production (NPP) is by marine plants (approximately 50 ± 28 GtC/year; Falkowski et al. 2004; Carr et al. 2006; Chavez et al. 2011). Phytoplankton NPP supports the biological pump, which transports 2–12 GtC/year of organic carbon to the deep sea (Doney 2010; Passow and Carlson 2012), where it is sequestered away from the atmospheric pool of carbon for 200–1,500 years. Since the ocean is an important carbon sink, climate-driven changes in NPP represent an important feedback because they potentially change atmospheric CO_2 abundance and forcing.

There are multiple links between RF-driven changes in climate, physical changes to the ocean and feedbacks to ocean carbon and heat uptake. Changes in ocean temperature, circulation and stratification driven by climate change alter phytoplankton NPP. Absorption of CO_2 by the ocean also increases its acidity, which can also affect NPP and therefore the carbon sink (see Ch. 13: Ocean Changes for a more detailed discussion of ocean acidification).

In addition to being an important carbon sink, the ocean dominates the hydrological cycle, since most surface evaporation and rainfall occur over the ocean (Trenberth et al. 2007; Schanze et al. 2010). The ocean component of the water vapor feedback derives from the rate of evaporation, which depends on surface wind stress and ocean temperature. Climate warming from radiative forcing also is associated with intensification of the water cycle (Ch. 7: Precipitation Change). Over decadal timescales the surface ocean salinity has increased in areas of high salinity, such as the subtropical gyres, and decreased in areas of low salinity, such as the Warm Pool region (see Ch. 13: Ocean Changes; Durack and Wijfels 2010; Good et al. 2013). This increase in stratification in select regions and mixing in other regions are feedback processes because they lead to altered patterns of ocean circulation, which impacts uptake of anthropogenic heat and CO_2.

Increased stratification inhibits surface mixing, high-latitude convection, and deep-water formation, thereby potentially weakening ocean circulations, in particular the Atlantic

FINAL DRAFT

Meridional Overturning Circulation (AMOC) (Andrews et al. 2012; Kostov et al. 2014; see also Ch. 13: Ocean Changes). Reduced deep-water formation and slower overturning are associated with decreased heat and carbon sequestration at greater depths. Observational evidence is mixed regarding whether the AMOC has slowed over the past decades to century (see Sect. 13.2.1 of Ch. 13: Ocean Changes). Future projections show that the strength of AMOC may significantly decrease as the ocean warms and freshens and as upwelling in the Southern Ocean weakens due to the storm track moving poleward (Rahmstorf et al. 2015; see also Ch. 13: Ocean Changes). Such a slowdown of the ocean currents will impact the rate at which the ocean absorbs CO_2 and heat from the atmosphere.

Increased ocean temperatures also accelerate ice sheet melt, particularly for the Antarctic Ice Sheet where basal sea ice melting is important relative to surface melting due to colder surface temperatures (Rignot and Thomas 2002). For the Greenland Ice Sheet, submarine melting at tidewater margins is also contributing to volume loss (van den Broeke et al. 2009). In turn, changes in ice sheet melt rates change cold- and freshwater inputs, also altering ocean stratification. This affects ocean circulation and the ability of the ocean to absorb more GHGs and heat (Enderlin and Hamilton 2014). Enhanced sea ice export to lower latitudes gives rise to local salinity anomalies (such as the Great Salinity Anomaly; Gelderloos et al. 2012) and therefore to changes in ocean circulation and air–sea exchanges of momentum, heat, and freshwater, which in turn affect the atmospheric distribution of heat and GHGs.

Remote sensing of sea surface temperature and chlorophyll as well as model simulations and sediment records suggest that global phytoplankton NPP may have increased recently as a consequence of decadal-scale natural climate variability, such as the El Niño–Southern Oscillation, which promotes vertical mixing and upwelling of nutrients (Bidigare et al. 2009; Chavez et al. 2011; Zhai et al. 2013). Analyses of longer trends, however, suggest that phytoplankton NPP has decreased by about 1% per year over the last 100 years (Behrenfeld et al. 2006; Boyce et al. 2010; Capotondi et al. 2012). The latter results, although controversial (Rykaczewski and Dunne 2011), are the only studies of the global rate of change over this period. In contrast, model simulations show decreases of only 6.6% in NPP and 8% in the biological pump over the last five decades (Laufkötter et al. 2015). Total NPP is complex to model, as there are still areas of uncertainty on how multiple physical factors affect phytoplankton growth, grazing, and community composition, and as certain phytoplankton species are more efficient at carbon export (Jin et al. 2006; Fu et al. 2016). As a result, model uncertainty is still significant in NPP projections (Frölicher et al. 2016). While there are variations across climate model projections, there is good agreement that in the future there will be increasing stratification, decreasing NPP, and a decreasing sink of CO_2 to the ocean via biological activity (Fu et al. 2016). Overall, compared to the 1990s, in 2090 total NPP is expected to decrease by 2%–16% and export production (that is, particulate flux to the deep ocean) could decline by 7%–18% (RCP 8.5; Fu et al. 2016). Consistent with this result, carbon cycle feedbacks in the ocean were positive (that is, higher CO_2 concentrations leading to a lower

FINAL DRAFT

rate of CO_2 sequestration to the ocean, thereby accelerating the growth of atmospheric CO_2 concentrations) across the suite of CMIP5 models.

PERMAFROST AND HYDRATES

Permafrost and methane hydrates contain large stores of methane and (for permafrost) carbon in the form of organic materials, mostly at northern high latitudes. With warming, this organic material can thaw, making previously frozen organic matter available for microbial decomposition, releasing CO_2 and methane to the atmosphere, providing additional radiative forcing and accelerating warming. This process defines the permafrost–carbon feedback. Combined data and modeling studies suggest that this feedback is *very likely* positive (Schaefer et al. 2014; Koven et al. 2015a; Schuur et al. 2015). This feedback was not included in recent IPCC projections but is an active area of research. Accounting for permafrost-carbon release reduces the amount of emissions allowable from anthropogenic sources in future GHG stabilization or mitigation scenarios (González-Eguino and Neumann 2016).

The permafrost–carbon feedback in the RCP8.5 emissions scenario (Section 1.2.2 and Figure 1.4) contributes 120 ± 85 Gt of additional carbon by 2100; this represents 6% of the total anthropogenic forcing for 2100 and corresponds to a global temperature increase of +0.52° ± 0.38°F (+0.29° ± 0.21°C) (Schaefer et al. 2014). Considering the broader range of forcing scenarios (Figure 1.4), it is *likely* that the permafrost–carbon feedback increases carbon emissions between 2% and 11% by 2100. A key feature of the permafrost feedback is that, once initiated, it will continue for an extended period because emissions from decomposition occur slowly over decades and longer. In the coming few decades, enhanced plant growth at high latitudes and its associated CO_2 sink (Friedlingstein et al. 2006) are expected to partially offset the increased emissions from permafrost thaw (Schaefer et al. 2014; Schuur et al. 2015); thereafter, decomposition will dominate uptake. Recent evidence indicates that permafrost thaw is occurring faster than expected; poorly understood deep-soil carbon decomposition and ice wedge processes *likely* contribute (Koven et al. 2015b; Liljedahl et al. 2016). Chapter 11: Arctic Changes includes a more detailed discussion of permafrost and methane hydrates in the Arctic. Future changes in permafrost emissions and the potential for even greater emissions from methane hydrates in the continental shelf are discussed further in Chapter 15: Potential Surprises.

FINAL DRAFT

TRACEABLE ACCOUNTS

Key Finding 1

Human activities continue to significantly affect Earth's climate by altering factors that change its radiative balance. These factors, known as radiative forcings, include changes in greenhouse gases, small airborne particles (aerosols), and the reflectivity of the Earth's surface. In the industrial era, human activities have been, and are increasingly, the dominant cause of climate warming. The increase in radiative forcing due to these activities has far exceeded the relatively small net increase due to natural factors, which include changes in energy from the sun and the cooling effect of volcanic eruptions. (*Very high confidence*)

Description of evidence base

The Key Finding and supporting text summarizes extensive evidence documented in the climate science literature, including in previous national (NCA3; Melillo et al. 2014) and international (IPCC 2013) assessments. The assertion that Earth's climate is controlled by its radiative balance is a well-established physical property of the planet. Quantification of the changes in Earth's radiative balance come from a combination of observations and calculations. Satellite data are used directly to observe changes in Earth's outgoing visible and infrared radiation. Since 2002, observations of incoming sunlight include both total solar irradiance and solar spectral irradiance (Ermolli et al. 2013). Extensive in situ and remote sensing data are used to quantify atmospheric concentrations of radiative forcing agents (greenhouse gases [e.g. Ciais et al. 2013; Le Quéré et al. 2016] and aerosols [e.g. Bond et al. 2013; Boucher et al. 2013; Myhre et al. 2013; Jiao et al. 2014; Tsigaridis et al. 2014; Koffi et al. 2016]) and changes in land cover (Zhu et al. 2016; Mao et al. 2016; Ju and Masek 2016), as well as the relevant properties of these agents (for example, aerosol microphysical and optical properties). Climate models are constrained by these observed concentrations and properties. Concentrations of long-lived greenhouse gases in particular are well-quantified with observations because of their relatively high spatial homogeneity. Climate model calculations of radiative forcing by greenhouse gases and aerosols are supported by observations of radiative fluxes from the surface, from airborne research platforms, and from satellites. Both direct observations and modeling studies show large, explosive eruptions affect climate parameters for years to decades (Robock 2000; Raible et al. 2016). Over the industrial era radiative forcing by volcanoes has been episodic and currently does not contribute significantly to forcing trends. Observations indicate a positive but small increase in solar input over the industrial era (Kopp 2014; Kopp et al. 2016; Myhre et al. 2013). Relatively higher variations in solar input at shorter (UV) wavelengths (Floyd et al. 2003) may be leading to indirect changes in Earth's radiative balance through their impact on ozone concentrations that are larger than the radiative impact of changes in total solar irradiance (Ermolli et al. 2013; Bolduc et al. 2015; Gray et al. 2010; Lockwood 2012; Seppälä et al. 2014), but these changes are also small in comparison to anthropogenic greenhouse gas and aerosol forcing (Myhre et al. 2013). The finding of an increasingly strong positive forcing over the industrial era is supported

FINAL DRAFT

by observed increases in atmospheric temperatures (see Ch. 1: Our Globally Changing Climate) and by observed increases in ocean temperatures (Ch. 1: Our Globally Changing Climate; Ch. 13: Ocean Changes). The attribution of climate change to human activities is supported by climate models, which are able to reproduce observed temperature trends when RF from human activities is included, and considerably deviate from observed trends when only natural forcings are included (Ch. 3: Detection and Attribution, Figure 3.1).

Major uncertainties

The largest source of uncertainty in radiative forcing (both natural and anthropogenic) over the industrial era is quantifying forcing by aerosols. This finding is consistent across previous assessments (e.g., IPCC 2007; IPCC 2013). The major uncertainties associated with aerosol forcing is discussed below in the Traceable Accounts for Key Finding 2.

Recent work has highlighted the potentially larger role of variations in UV solar irradiance, versus total solar irradiance, in solar forcing. However, this increase in solar forcing uncertainty is not sufficiently large to reduce confidence that anthropogenic activities dominate industrial-era forcing.

Assessment of confidence based on evidence and agreement, including short description of nature of evidence and level of agreement

There is *very high confidence* that anthropogenic radiative forcing exceeds natural forcing over the industrial era based on quantitative assessments of known radiative forcing components. Assessments of the natural forcings of solar irradiance changes and volcanic activity show with *very high confidence* that both forcings are small over the industrial era relative to total anthropogenic forcing. Total anthropogenic forcing is assessed to have become larger and more positive during the industrial era, while natural forcings show no similar trend.

Summary sentence or paragraph that integrates the above information

This key finding is consistent with that in the IPCC Fourth Assessment Report (AR4) (IPCC 2007) and Fifth Assessment Report (AR5) (IPCC 2013); namely, anthropogenic radiative forcing is positive (climate warming) and substantially larger than natural forcing from variations in solar input and volcanic emissions. Confidence in this finding has increased from AR4 to AR5, as anthropogenic GHG forcings have continued to increase, whereas solar forcing remains small and volcanic forcing near-zero over decadal timescales.

FINAL DRAFT

Key Finding 2

Aerosols caused by human activity play a profound and complex role in the climate system through radiative effects in the atmosphere and on snow and ice surfaces and through effects on cloud formation and properties. The combined forcing of aerosol–radiation and aerosol–cloud interactions is negative (cooling) over the industrial era (*high confidence*), offsetting a substantial part of greenhouse gas forcing, which is currently the predominant human contribution. The magnitude of this offset, globally averaged, has declined in recent decades, despite increasing trends in aerosol emissions or abundances in some regions. (*Medium to high confidence*)

Description of evidence base

The Key Finding and supporting text summarize extensive evidence documented in the climate science literature, including in previous national (NCA3; Melillo et al. 2014) and international (IPCC 2013) assessments. Aerosols affect the Earth's albedo by directly interacting with solar radiation (scattering and absorbing sunlight) and by affecting cloud properties (albedo and lifetime).

Fundamental physical principles show how atmospheric aerosols scatter and absorb sunlight (aerosol–radiation interaction), and thereby directly reduce incoming solar radiation reaching the surface. Extensive in situ and remote sensing data are used to measure emission of aerosols and aerosol precursors from specific source types, the concentrations of aerosols in the atmosphere, aerosol microphysical and optical properties, and, via remote sensing, their direct impacts on radiative fluxes. Atmospheric models used to calculate aerosol forcings are constrained by these observations (see Key Finding #1).

In addition to their direct impact on radiative fluxes, aerosols also act as cloud condensation nuclei. Aerosol–cloud interactions are more complex, with a strong theoretical basis supported by observational evidence. Multiple observational and modeling studies have concluded that increasing the number of aerosols in the atmosphere increases cloud albedo and lifetime, adding to the negative forcing (aerosol–cloud microphysical interactions) (e.g., Twohy 2005; Lohmann and Feichter 2005; Quaas et al. 2009; Rosenfeld et al. 2014). Particles that absorb sunlight increase atmospheric heating; if they are sufficiently absorbing, the net effect of scattering plus absorption is a positive radiative forcing. Only a few source types (for example, from diesel engines) produce aerosols that are sufficiently absorbing that they have a positive radiative forcing (Bond et al. 2013). Modeling studies, combined with observational inputs, have investigated the thermodynamic response to aerosol absorption in the atmosphere. Averaging over aerosol locations relative to the clouds and other factors, the resulting changes in cloud properties represent a negative forcing, offsetting approximately 15% of the positive radiative forcing from heating by absorbing aerosols (specifically, black carbon) (Bond et al. 2013).

Modeling and observational evidence both show that annually averaged global aerosol ERF increased until the 1980's and since then has flattened or slightly declined (Wild 2009; Szopa et

FINAL DRAFT

al. 2013; Stjern and Krisjansson 2015; Wang et al. 2015), driven by the introduction of stronger air quality regulations (Smith and Bond 2014; Fiore et al. 2015). In one recent study (Myhre et al. 2017), global-mean aerosol RF has become more less negative since IPCC AR5 (Myhre et al. 2013), due to a combination of declining sulfur dioxide emissions (which produce negative RF) and increasing black carbon emissions (which produce positive RF). Within these global trends there are significant regional variations (e.g., Mao et al. 2014), driven by both changes in aerosol abundance and changes in the relative contributions of primarily light-scattering and light-absorbing aerosols (Fiore et al. 2015; Myhre et al. 2017). In Europe and North America, aerosol ERF has significantly declined (become less negative) since the 1980s (Marmer et al. 2007; Philipona et al. 2009; Murphy et al. 2011; Leibensperger et al. 2012; Kühn et al. 2014; Turnock et al. 2015). In contrast, observations show significant increases in aerosol abundances over India (Babu et al. 2013; Krishna Moorthy et al. 2013), and these increases are expected to continue into the near future (Pietikainen et al. 2015). Several modeling and observational studies point to aerosol ERF for China peaking around 1990 (Streets et al. 2008; Li et al. 2013; Wang et al. 2013), though in some regions of China aerosol abundances and ERF have continued to increase (Wang et al. 2013). The suite of emissions scenarios used for future climate projection (i.e., the scenarios shown in Ch. 1: Our Globally Changing Climate, Figure 1.4) includes emissions for aerosols and aerosol precursors. Across this range of scenarios, globally averaged ERF of aerosols is expected to decline (become less negative) in the coming decades (Szopa et al. 2013; Smith and Bond 2014), reducing the current aerosol offset to the increasing RF from GHGs.

Major uncertainties

Aerosol–cloud interactions are the largest source of uncertainty in both aerosol and total anthropogenic radiative forcing. These include the microphysical effects of aerosols on clouds and changes in clouds that result from the rapid response to absorption of sunlight by aerosols. This finding, consistent across previous assessments (e.g., Forster et al. 2007; Myhre et al. 2013), is due to poor understanding of how both natural and anthropogenic aerosol emissions have changed and how changing aerosol concentrations and composition affect cloud properties (albedo and lifetime) (Boucher et al. 2013; Carslaw et al. 2013). From a theoretical standpoint, aerosol–cloud interactions are complex, and using observations to isolate the effects of aerosols on clouds is complicated by the fact that other factors (for example, the thermodynamic state of the atmosphere) also strongly influence cloud properties. Further, changes in aerosol properties and the atmospheric thermodynamic state are often correlated and interact in non-linear ways (Stevens and Feingold 2009).

Assessment of confidence based on evidence and agreement, including short description of nature of evidence and level of agreement

There is *very high confidence* that aerosol radiative forcing is negative on a global, annually averaged basis, *medium confidence* in the magnitude of the aerosol RF, *high* confidence that aerosol ERF is also, on average, negative, and *low to medium confidence* in the magnitude of

FINAL DRAFT

aerosol ERF. Lower confidence in the magnitude of aerosol ERF is due to large uncertainties in the effects of aerosols on clouds. Combined, we assess a *high level of confidence* that aerosol ERF is negative and sufficiently large to be substantially offsetting positive GHG forcing. Improvements in the quantification of emissions, in observations (from both surface-based networks and satellites), and in modeling capability give *medium* to *high confidence* in the finding that aerosol forcing trends are decreasing in recent decades.

Summary sentence or paragraph that integrates the above information

This key finding is consistent with the findings of IPCC AR5 (Myhre et al. 2013) that aerosols constitute a negative radiative forcing. While significant uncertainty remains in the quantification of aerosol ERF, we assess with *high confidence* that aerosols offset about half of the positive forcing by anthropogenic CO_2 and about a third of the forcing by all well-mixed anthropogenic GHGs. The fraction of GHG forcing that is offset by aerosols has been decreasing over recent decades, as aerosol forcing has leveled off while GHG forcing continues to increase.

Key Finding 3

The interconnected Earth–atmosphere–ocean climate system includes a number of positive and negative feedback processes that can either strengthen (positive feedback) or weaken (negative feedback) the system's responses to human and natural influences. These feedbacks operate on a range of timescales from very short (essentially instantaneous) to very long (centuries). Global warming by net radiative forcing over the industrial era includes a substantial amplification from these feedbacks (approximately a factor of three) (*high confidence*). While there are large uncertainties associated with some of these feedbacks, the net feedback effect over the industrial era has been positive (amplifying warming) and will continue to be positive in coming decades. (*Very high confidence*)

Description of evidence base

The variety of climate system feedbacks all depend on fundamental physical principles and are known with a range of uncertainties. The Planck feedback is based on well-known radiative transfer models. The largest positive feedback is the water vapor feedback, which derives from the dependence of vapor pressure on temperature. There is *very high confidence* that this feedback is positive, approximately doubling the direct forcing due to CO_2 emissions alone. The lapse rate feedback derives from thermodynamic principles. There is *very high confidence* that this feedback is negative and partially offsets the water vapor feedback. The water vapor and lapse-rate feedbacks are linked by the fact that both are driven by increases in atmospheric water vapor with increasing temperature. Estimates of the magnitude of these two feedbacks have changed little across recent assessments (Randall et al. 2007; Boucher et al. 2013). The snow– and ice–albedo feedback is positive in sign, with the magnitude of the feedback dependent in part

FINAL DRAFT

on the timescale of interest (Hall and Qu 2006; Fernandes et al. 2009). The assessed strength of this feedback has also not changed significantly since IPCC (2007). Cloud feedbacks modeled using microphysical principles are either positive or negative, depending on the sign of the change in clouds with warming (increase or decrease) and the type of cloud that changes (low or high clouds). Recent international assessments (Randall et al. 2007; Boucher et al. 2013) and a separate feedback assessment (Vial et al. 2013) all give best estimates of the cloud feedback as net positive. Feedback via changes in atmospheric composition is not well-quantified, but is expected to be small relative to water-vapor-plus-lapse-rate, snow, and cloud feedbacks at the global scale (Raes et al. 2010). Carbon cycle feedbacks through changes in the land biosphere are currently of uncertain sign, and have asymmetric uncertainties: they might be small and negative but could also be large and positive (Seppälä 2009). Recent best estimates of the ocean carbon-cycle feedback are that it is positive with significant uncertainty that includes the possibility of a negative feedback for present-day CO_2 levels (Laufkötter et al. 2015; Steinacher et al. 2010). The permafrost–carbon feedback is *very likely* positive, and as discussed in Chapter 15: Potential Surprises, could be a larger positive feedback in the longer term. Thus, in the balance of multiple negative and positive feedback processes, the preponderance of evidence is that positive feedback processes dominate the overall radiative forcing feedback from anthropogenic activities.

Major uncertainties

Uncertainties in cloud feedbacks are the largest source of uncertainty in the net climate feedback (and therefore climate sensitivity) on the decadal to century time-scale (Boucher et al. 2013; Vial et al. 2013). This results from the fact cloud feedbacks can be either positive or negative, depending not only on the direction of change (more or less cloud) but also on the type of cloud affected and, to a lesser degree, the location of the cloud (Vial et al. 2013). On decadal and longer timescales, the biological and physical responses of the ocean and land to climate change, and the subsequent changes in land and oceanic sinks of CO_2, contribute significant uncertainty to the net climate feedback (Ch. 13: Ocean Changes). Changes in the Brewer-Dobson atmospheric circulation driven by climate change and subsequent effects on stratosphere–troposphere coupling also contribute to climate feedback uncertainty (Hauglustaine et al. 2005; Jiang et al. 2007; Li et al. 2008; Shepherd and McLandress 2011; Collins et al. 2013; McLandress et al. 2014).

Assessment of confidence based on evidence and agreement, including short description of nature of evidence and level of agreement

There is *high confidence* that the net effect of all feedback processes in the climate system is positive, thereby amplifying warming. This confidence is based on consistency across multiple assessments, including IPCC AR5 (IPCC 2013 and references therein), of the magnitude of, in particular, the largest feedbacks in the climate system, two of which (water vapor feedback and snow/ice albedo feedback) are definitively positive in sign. While significant increases in low

FINAL DRAFT

cloud cover with climate warming would be a large negative feedback to warming, modeling and observational studies do not support the idea of increases, on average, in low clouds with climate warming.

Summary sentence or paragraph that integrates the above information

The net effect of all identified feedbacks to forcing is positive based on the best current assessments and therefore amplifies climate warming. Feedback uncertainties, which are large for some processes, are included in these assessments. The various feedback processes operate on different timescales with carbon cycle and snow– and ice–albedo feedbacks operating on longer timelines than water vapor, lapse rate, cloud, and atmospheric composition feedbacks.

FINAL DRAFT

TABLES

Table 2.1. Global mean RF and ERF values in 2011 for the industrial era [a]

Radiative Forcing Term	Radiative forcing (W/m^2)	Effective radiative forcing (W/m^2) [b]
Well-mixed greenhouse gases (CO_2, CH_4, N_2O, and halocarbons)	+2.83 (2.54 to 3.12)	+2.83 (2.26 to 3.40)
Tropospheric ozone	+0.40 (0.20 to 0.60)	
Stratospheric ozone	–0.05 (–0.15 to +0.05)	
Stratospheric water vapor from CH_4	+0.07 (+0.02 to +0.12)	
Aerosol–radiation interactions	–0.35 (–0.85 to +0.15)	–0.45 (–0.95 to +0.05)
Aerosol–cloud interactions	Not quantified	–0.45 (–1.2 to 0.0)
Surface albedo (land use)	–0.15 (–0.25 to –0.05)	
Surface albedo (black carbon aerosol on snow and ice)	+0.04 (+0.02 to +0.09)	
Contrails	+0.01 (+0.005 to +0.03)	
Combined contrails and contrail-induced cirrus	Not quantified	+0.05 (0.02 to 0.15)
Total anthropogenic	Not quantified	+2.3 (1.1 to 3.3)
Solar irradiance	+0.05 (0.0 to +0.10)	

[a] From IPCC (Myhre et al. 2013)

[b] RF is a good estimate of ERF for most forcing agents except black carbon on snow and ice and aerosol–cloud interactions.

FINAL DRAFT

FIGURES

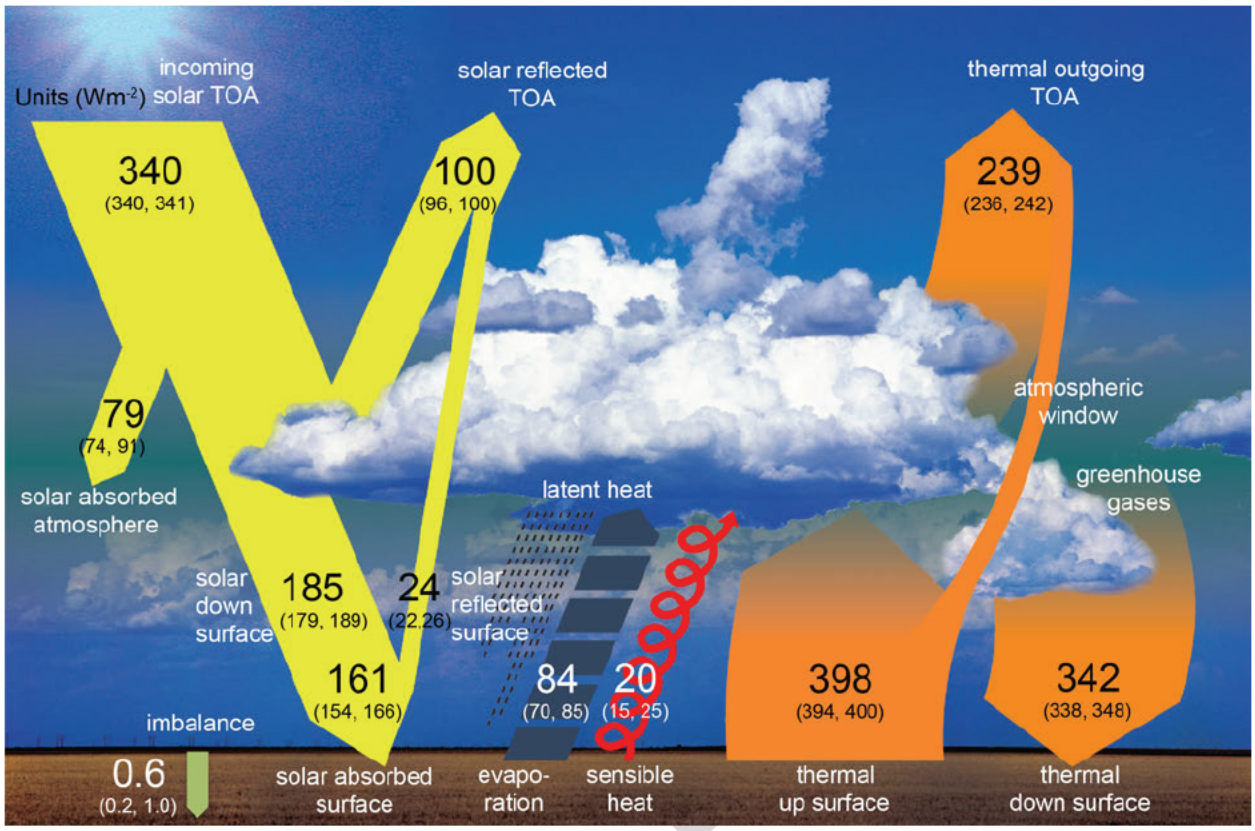

Figure 2.1: Global mean energy budget of the Earth under present-day climate conditions. Numbers state magnitudes of the individual energy fluxes in watts per square meter (W/m^2) averaged over Earth's surface, adjusted within their uncertainty ranges to balance the energy budgets of the atmosphere and the surface. Numbers in parentheses attached to the energy fluxes cover the range of values in line with observational constraints. Fluxes shown include those resulting from feedbacks. Note the net imbalance of 0.6 W/m^2 in the global mean energy budget. The observational constraints are largely provided by satellite-based observations, which have directly measured solar and infrared fluxes at the top of the atmosphere over nearly the whole globe since 1984 (Barkstrom 1984; Smith et al. 1994). More advanced satellite-based measurements focusing on the role of clouds in Earth's radiative fluxes have been available since 1998 (Wielicki et al. 1995, 1996). Top of Atmosphere (TOA) reflected solar values given here are based on observations 2001–2010; TOA outgoing longwave is based on 2005–2010 observations. (Figure source: Hartmann et al. 2013 Figure 2-11; © IPCC, used with permission).

FINAL

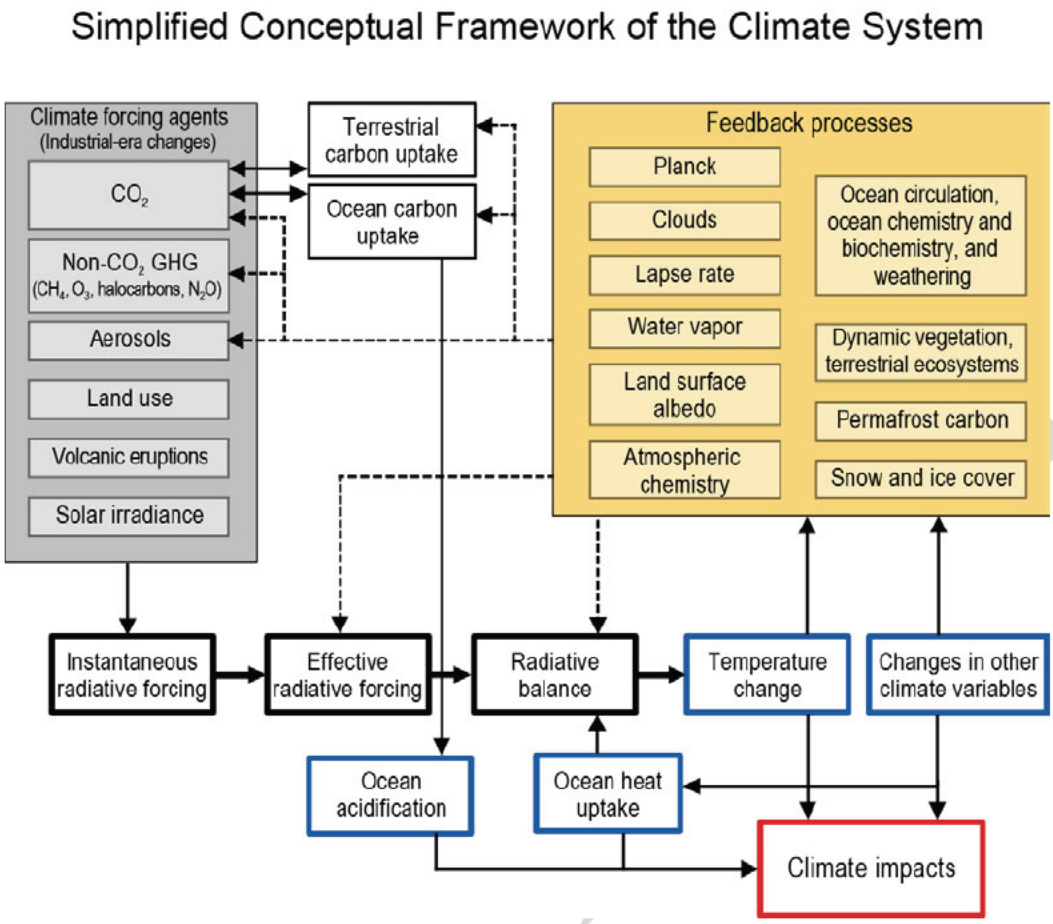

Figure 2.2: Simplified conceptual modeling framework for the climate system as implemented in many climate models (Ch. 4: Projections). Modeling components include forcing agents, feedback processes, carbon uptake processes, and radiative forcing and balance. The lines indicate physical interconnections (solid lines) and feedback pathways (dashed lines). Principal changes (blue boxes) lead to climate impacts (red box) and feedbacks. (Figure source: adapted from Knutti and Rugenstein 2015).

FINAL

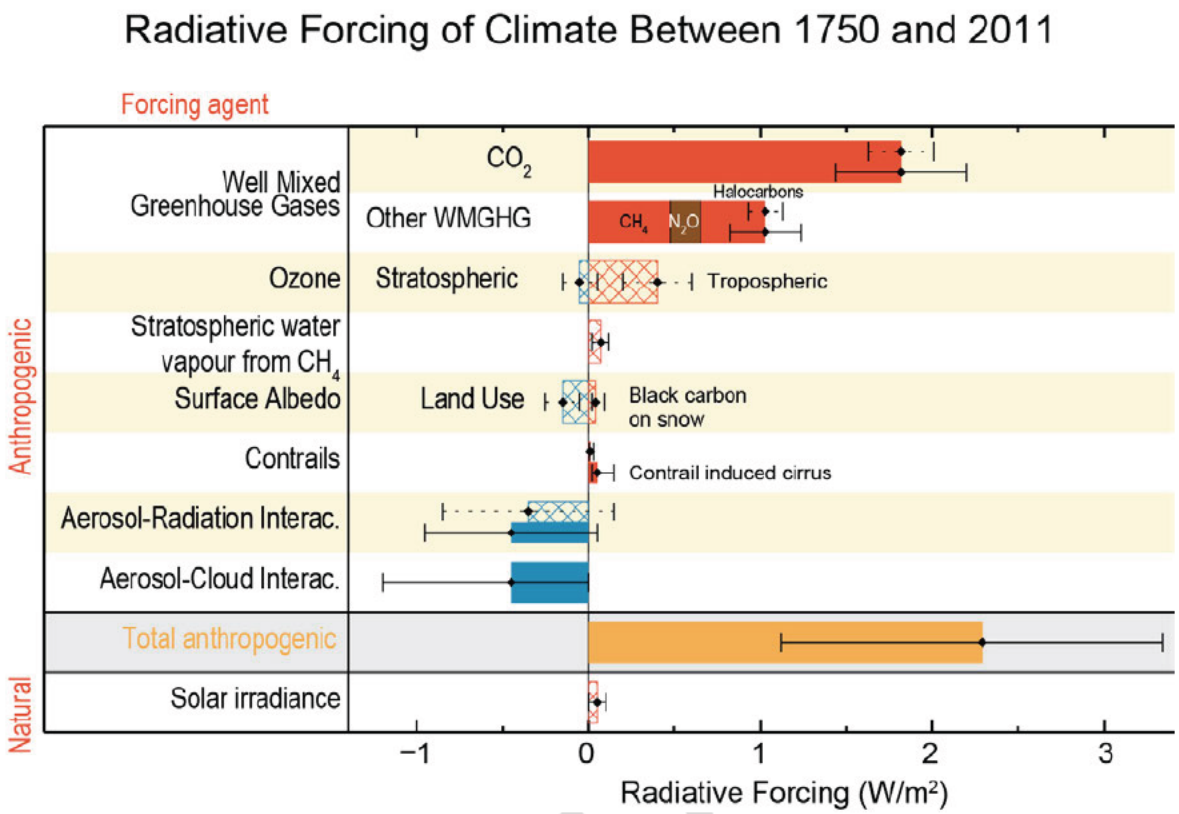

Figure 2.3: Bar chart for radiative forcing (RF; hatched) and effective radiative forcing (ERF; solid) for the period 1750–2011, where the total ERF is derived from the Intergovernmental Panel on Climate Change's Fifth Assessment Report. Uncertainties (5% to 95% confidence range) are given for RF (dotted lines) and ERF (solid lines). Volcanic forcing is not shown because this forcing is intermittent, exerting forcing over only a few years for eruptions during the industrial era; the net forcing over the industrial era is negligible. (Figure source: Myhre et al. 2013 Figure 8-15; © IPCC, used with permission).

FINAL

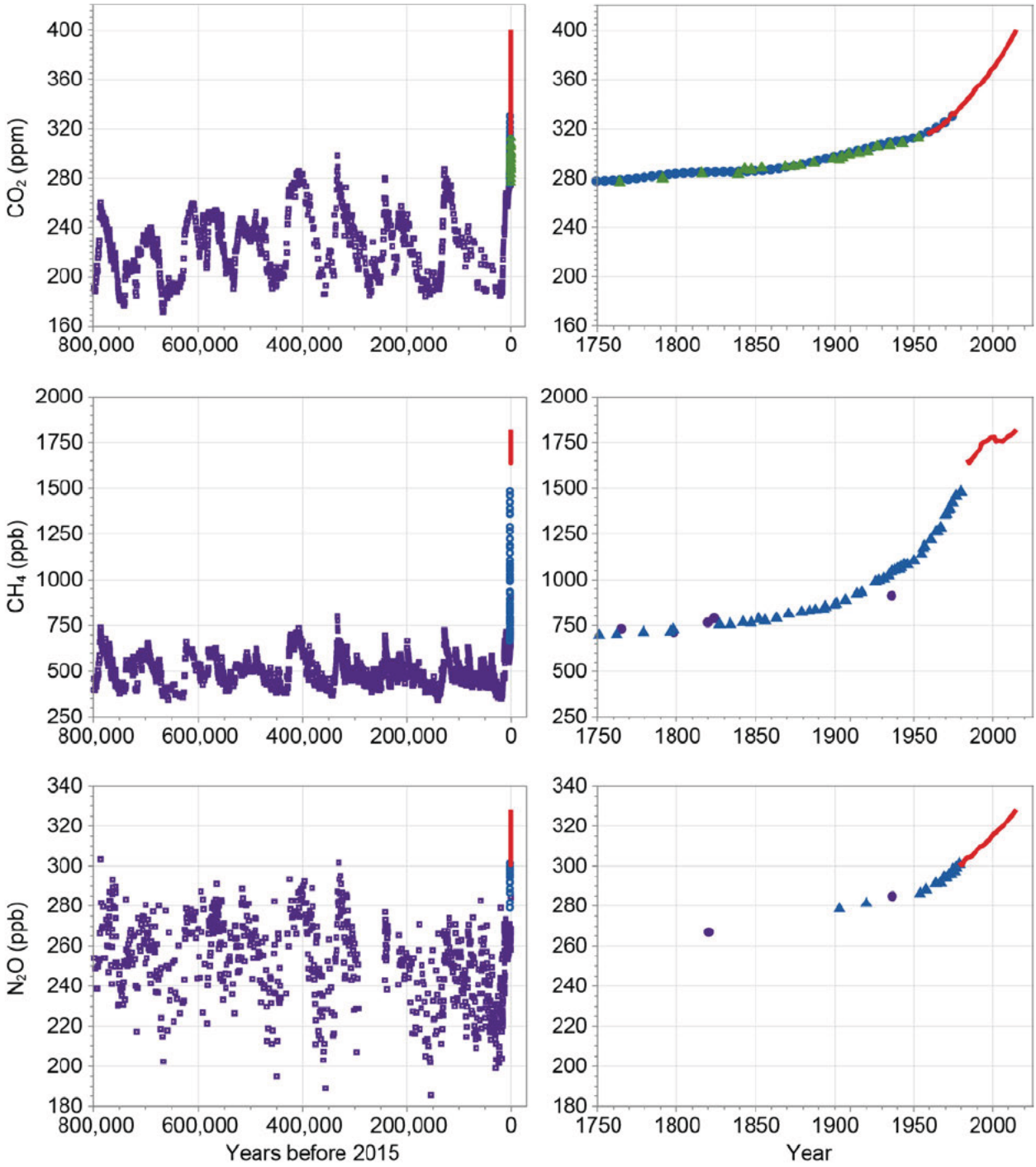

Figure 2.4: Atmospheric concentrations of CO_2 (top), CH_4 (middle), and N_2O (bottom) over the last 800,000 years (left panels) and for 1750–2015 (right panels). Measurements are shown from ice cores (symbols with different colors for different studies) and for direct atmospheric measurements (red lines). (Adapted from IPCC [2007], Figure SPM.1, © IPCC, used with permission; data are from https://www.epa.gov/climate-indicators/climate-change-indicators-atmospheric-concentrations-greenhouse-gases).

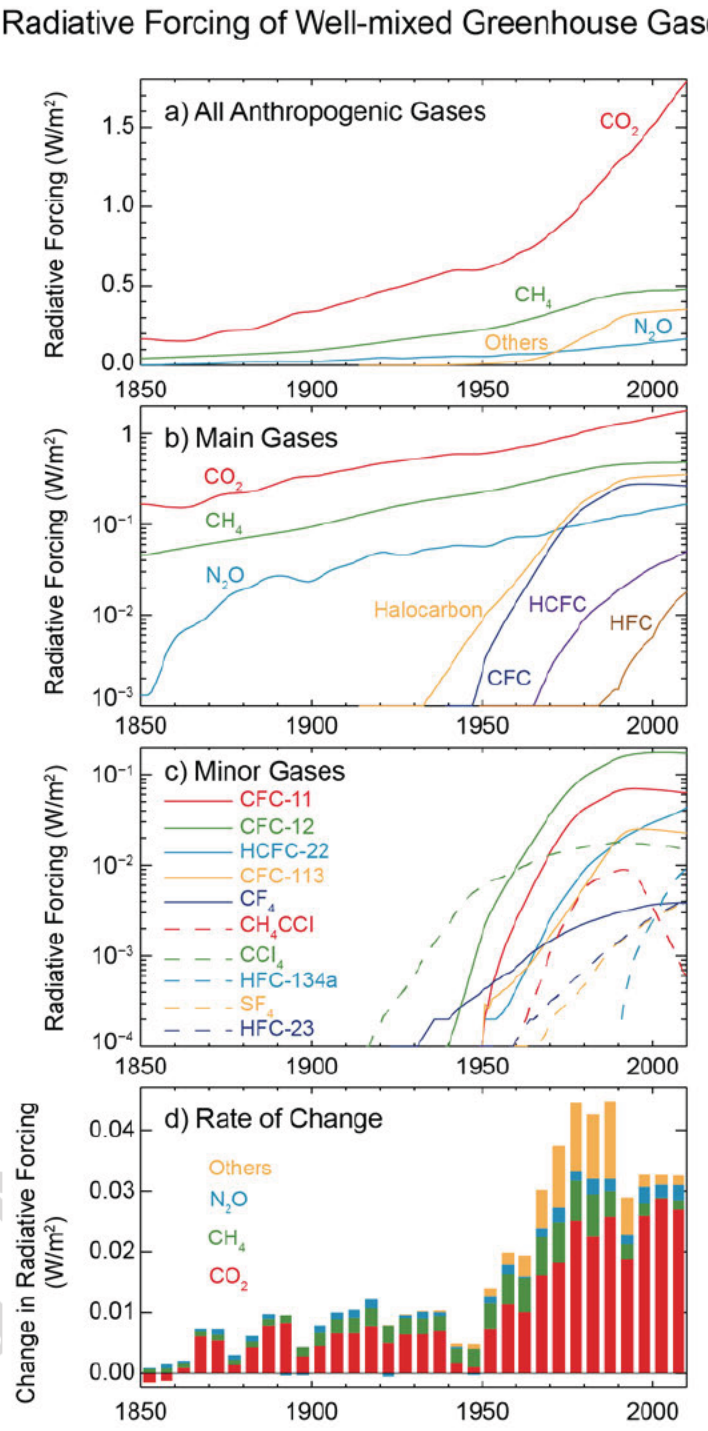

Figure 2.5: (a) Radiative forcing (RF) from the major WMGHGs and groups of halocarbons (Others) from 1850 to 2011; (b) the data in (a) with a logarithmic scale; (c) RFs from the minor WMGHGs from 1850 to 2011 (logarithmic scale); (d) the annual rate of change ([W/m^2]/year) in forcing from the major WMGHGs and halocarbons from 1850 to 2011. (Figure source: Myhre et al. 2013, Figure 8-06; © IPCC, used with permission).

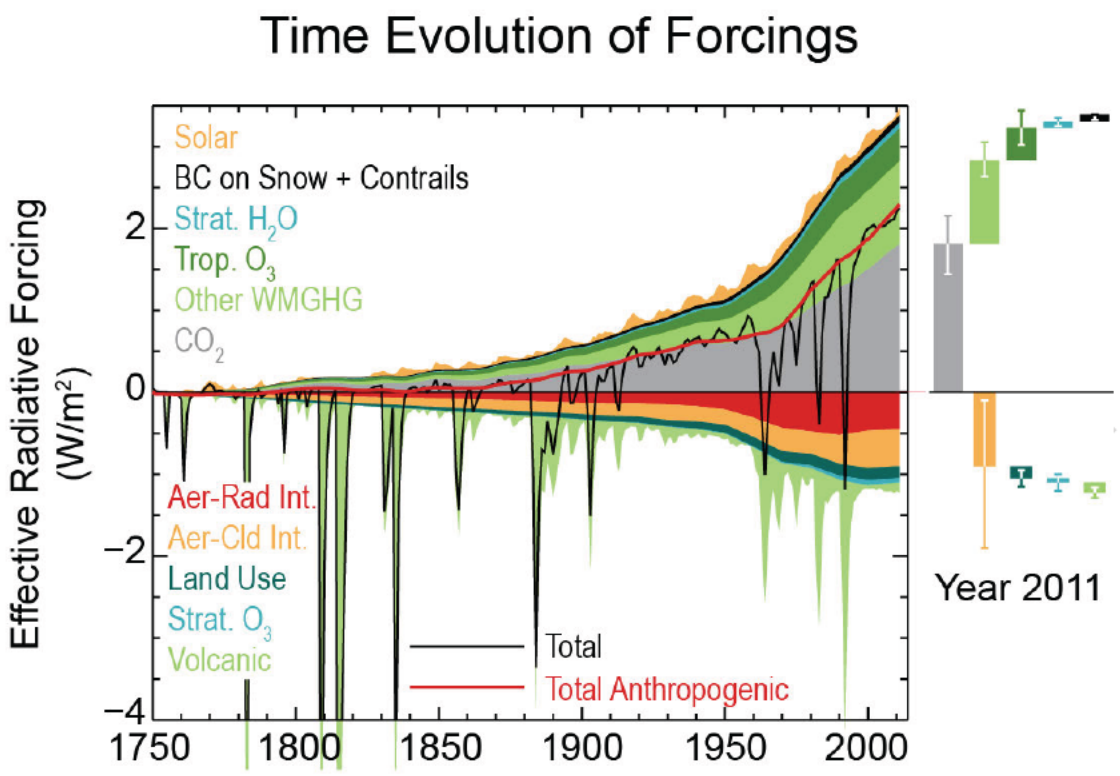

Figure 2.6: Changes in effective radiative forcing across the industrial era for anthropogenic and natural forcing mechanisms. Also shown are the sum of all forcings (Total; black line) and the sum of anthropogenic forcings (Total Anthropogenic; red line). Forcing due to changes in surface albedo through black carbon in snow ("BC on snow") and forcing by contrails are grouped together in the plot. Bars with the forcing and uncertainty ranges (5% to 95% confidence range) at present (as of 2011) are given on the right side of the figure. For aerosols, the sum of ERF from aerosol–radiation interaction ("Aer–Rad Int.") and aerosol–cloud ("Aer–Cld Int.") are shown as a single orange bar to the right. The uncertainty ranges are for the change between 1750 and 2011 (Table 8.6). For aerosols, only the uncertainty in the total aerosol ERF is given, as noted above. For several of the forcing agents the relative uncertainty may be larger for certain time periods compared to present. See the Intergovernmental Panel on Climate Change Fifth Assessment Report (IPCC AR5) Supplementary Material Table 8.SM.8 (Myhre et al. 2013) for further information on the forcing time evolutions. Forcing numbers are provided in Annex II of IPCC AR5. The total anthropogenic forcing was 0.57 (0.29 to 0.85) W/m^2 in 1950, 1.25 (0.64 to 1.86) W/m^2 in 1980, and 2.29 (1.13 to 3.33) W/m^2 in 2011. (Figure source: Myhre et al. 2013, Figure 8-18; © IPCC, used with permission).

FINAL D

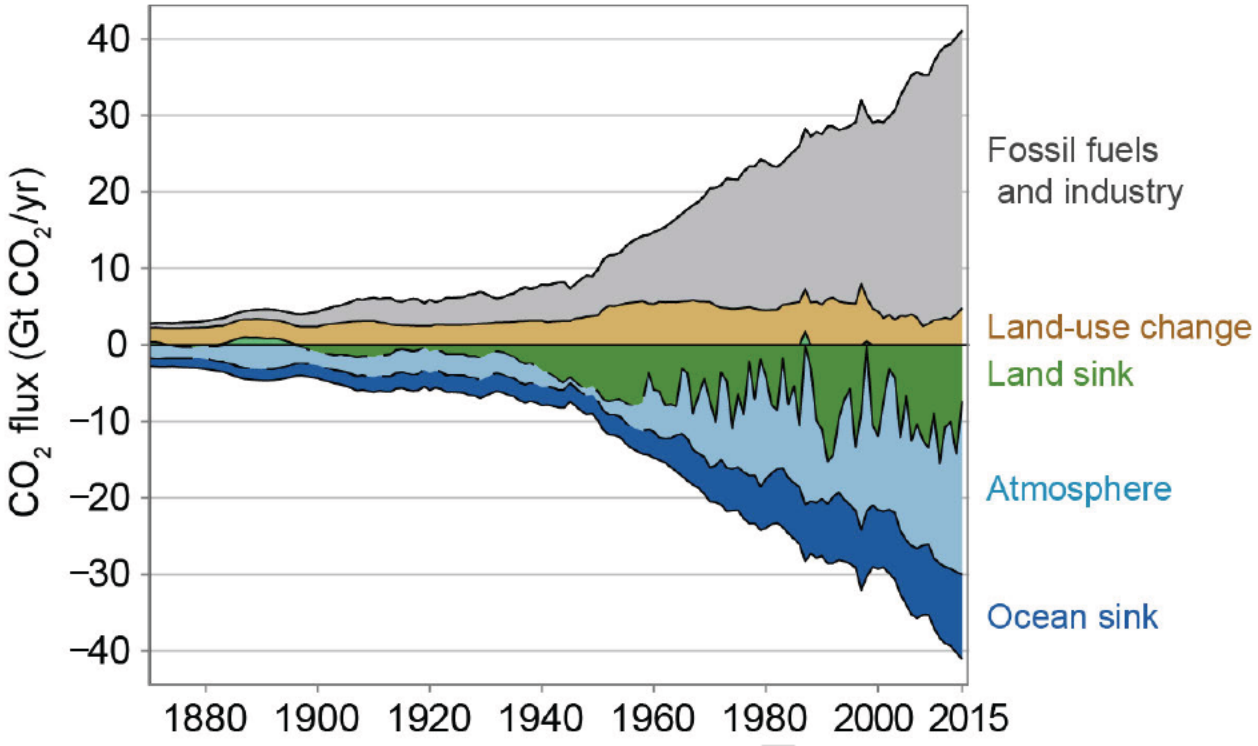

Figure 2.7: CO_2 sources and sinks ($GtCO_2$/yr) over the period 1870–2015. The partitioning of atmospheric emissions among the atmosphere, land, and ocean is shown as equivalent negative emissions in the lower panel; of these, the land and ocean terms are sinks of atmospheric CO_2. CO_2 emissions from net land-use changes are mainly from deforestation. The atmospheric CO_2 growth rate is derived from atmospheric observations and ice core data. The ocean CO_2 sink is derived from a combination of models and observations. The land sink is the residual of the other terms in a balanced CO_2 budget and represents the sink of anthropogenic CO_2 in natural land ecosystems. These terms only represent changes since 1750 and do not include natural CO_2 fluxes (for example, from weathering and outgassing from lakes and rivers). (Figure source: Le Quére et al. 2016, Figure 3).

FINAL

REFERENCES

ACC-MIP, 2017: Atmospheric Chemistry and Climate MIP. WCRP Working Group on Coupled Modeling. https://www.wcrp-climate.org/modelling-wgcm-mip-catalogue/modelling-wgcm-mips-2/226-modelling-wgcm-acc-mip.

Allen, M.R. and W.J. Ingram, 2002: Constraints on future changes in climate and the hydrologic cycle. *Nature,* **419,** 224-232. http://dx.doi.org/10.1038/nature01092

Alley, K.E., T.A. Scambos, M.R. Siegfried, and H.A. Fricker, 2016: Impacts of warm water on Antarctic ice shelf stability through basal channel formation. *Nature Geoscience,* **9,** 290-293. http://dx.doi.org/10.1038/ngeo2675

Anav, A., P. Friedlingstein, M. Kidston, L. Bopp, P. Ciais, P. Cox, C. Jones, M. Jung, R. Myneni, and Z. Zhu, 2013: Evaluating the land and ocean components of the global carbon cycle in the CMIP5 earth system models. *Journal of Climate,* **26,** 6801-6843. http://dx.doi.org/10.1175/jcli-d-12-00417.1

Andrews, T., J.M. Gregory, M.J. Webb, and K.E. Taylor, 2012: Forcing, feedbacks and climate sensitivity in CMIP5 coupled atmosphere-ocean climate models. *Geophysical Research Letters,* **39,** L09712. http://dx.doi.org/10.1029/2012GL051607

Andronova, N.G., E.V. Rozanov, F. Yang, M.E. Schlesinger, and G.L. Stenchikov, 1999: Radiative forcing by volcanic aerosols from 1850 to 1994. *Journal of Geophysical Research: Atmospheres,* **104,** 16807-16826.

Babu, S.S., M.R. Manoj, K.K. Moorthy, M.M. Gogoi, V.S. Nair, S.K. Kompalli, S.K. Satheesh, K. Niranjan, K. Ramagopal, P.K. Bhuyan, and D. Singh, 2013: Trends in aerosol optical depth over Indian region: Potential causes and impact indicators. *Journal of Geophysical Research: Atmospheres,* **118,** 11,794-11,806. http://dx.doi.org/10.1002/2013JD020507

Banerjee, A., A.T. Archibald, A.C. Maycock, P. Telford, N.L. Abraham, X. Yang, P. Braesicke, and J.A. Pyle, 2014: Lightning NO_x, a key chemistry–climate interaction: Impacts of future climate change and consequences for tropospheric oxidising capacity. *Atmospheric Chemistry and Physics,* **14,** 9871-9881. http://dx.doi.org/10.5194/acp-14-9871-2014

Barkstrom, B.R., 1984: The Earth Radiation Budget Experiment (ERBE). *Bulletin of the American Meteorological Society,* **65,** 1170-1185. http://dx.doi.org/10.1175/1520-0477(1984)065<1170:terbe>2.0.co;2

Behrenfeld, M.J., R.T. O'Malley, D.A. Siegel, C.R. McClain, J.L. Sarmiento, G.C. Feldman, A.J. Milligan, P.G. Falkowski, R.M. Letelier, and E.S. Boss, 2006: Climate-driven trends in contemporary ocean productivity. *Nature,* **444,** 752-755. http://dx.doi.org/10.1038/nature05317

FINAL DRAFT

Bidigare, R.R., F. Chai, M.R. Landry, R. Lukas, C.C.S. Hannides, S.J. Christensen, D.M. Karl, L. Shi, and Y. Chao, 2009: Subtropical ocean ecosystem structure changes forced by North Pacific climate variations. *Journal of Plankton Research,* **31,** 1131-1139. http://dx.doi.org/10.1093/plankt/fbp064

Bindoff, N.L., P.A. Stott, K.M. AchutaRao, M.R. Allen, N. Gillett, D. Gutzler, K. Hansingo, G. Hegerl, Y. Hu, S. Jain, I.I. Mokhov, J. Overland, J. Perlwitz, R. Sebbari, and X. Zhang, 2013: Detection and attribution of climate change: From global to regional. *Climate Change 2013: The Physical Science Basis. Contribution of Working Group I to the Fifth Assessment Report of the Intergovernmental Panel on Climate Change*. Stocker, T.F., D. Qin, G.-K. Plattner, M. Tignor, S.K. Allen, J. Boschung, A. Nauels, Y. Xia, V. Bex, and P.M. Midgley, Eds. Cambridge University Press, Cambridge, United Kingdom and New York, NY, USA, 867–952. http://www.climatechange2013.org/report/full-report/

Boer, G. and B. Yu, 2003: Climate sensitivity and response. *Climate Dynamics,* **20,** 415-429. http://dx.doi.org/10.1007/s00382-002-0283-3

Bolduc, C., M.S. Bourqui, and P. Charbonneau, 2015: A comparison of stratospheric photochemical response to different reconstructions of solar ultraviolet radiative variability. *Journal of Atmospheric and Solar-Terrestrial Physics,* **132,** 22-32. http://dx.doi.org/10.1016/j.jastp.2015.06.008

Bond, T.C., S.J. Doherty, D.W. Fahey, P.M. Forster, T. Berntsen, B.J. DeAngelo, M.G. Flanner, S. Ghan, B. Kärcher, D. Koch, S. Kinne, Y. Kondo, P.K. Quinn, M.C. Sarofim, M.G. Schultz, M. Schulz, C. Venkataraman, H. Zhang, S. Zhang, N. Bellouin, S.K. Guttikunda, P.K. Hopke, M.Z. Jacobson, J.W. Kaiser, Z. Klimont, U. Lohmann, J.P. Schwarz, D. Shindell, T. Storelvmo, S.G. Warren, and C.S. Zender, 2013: Bounding the role of black carbon in the climate system: A scientific assessment. *Journal of Geophysical Research: Atmospheres,* **118,** 5380-5552. http://dx.doi.org/10.1002/jgrd.50171

Bony, S., R. Colman, V.M. Kattsov, R.P. Allan, C.S. Bretherton, J.-L. Dufresne, A. Hall, S. Hallegatte, M.M. Holland, W. Ingram, D.A. Randall, B.J. Soden, G. Tselioudis, and M.J. Webb, 2006: How well do we understand and evaluate climate change feedback processes? *Journal of Climate,* **19,** 3445-3482. http://dx.doi.org/10.1175/JCLI3819.1

Boucher, O., D. Randall, P. Artaxo, C. Bretherton, G. Feingold, P. Forster, V.-M. Kerminen, Y. Kondo, H. Liao, U. Lohmann, P. Rasch, S.K. Satheesh, S. Sherwood, B. Stevens, and X.Y. Zhang, 2013: Clouds and aerosols. *Climate Change 2013: The Physical Science Basis. Contribution of Working Group I to the Fifth Assessment Report of the Intergovernmental Panel on Climate Change*. Stocker, T.F., D. Qin, G.-K. Plattner, M. Tignor, S.K. Allen, J. Boschung, A. Nauels, Y. Xia, V. Bex, and P.M. Midgley, Eds. Cambridge University Press, Cambridge, United Kingdom and New York, NY, USA, 571–658. http://www.climatechange2013.org/report/full-report/

FINAL DRAFT

Boyce, D.G., M.R. Lewis, and B. Worm, 2010: Global phytoplankton decline over the past century. *Nature,* **466,** 591-596. http://dx.doi.org/10.1038/nature09268

Brzostek, E.R., J.B. Fisher, and R.P. Phillips, 2014: Modeling the carbon cost of plant nitrogen acquisition: Mycorrhizal trade-offs and multipath resistance uptake improve predictions of retranslocation. *Journal of Geophysical Research: Biogeosciences,* **119,** 1684-1697. http://dx.doi.org/10.1002/2014JG002660

Burkhardt, U. and B. Kärcher, 2011: Global radiative forcing from contrail cirrus. *Nature Climate Change,* **1,** 54-58. http://dx.doi.org/10.1038/nclimate1068

Capotondi, A., M.A. Alexander, N.A. Bond, E.N. Curchitser, and J.D. Scott, 2012: Enhanced upper ocean stratification with climate change in the CMIP3 models. *Journal of Geophysical Research: Oceans,* **117,** C04031. http://dx.doi.org/10.1029/2011JC007409

Carr, M.-E., M.A.M. Friedrichs, M. Schmeltz, M. Noguchi Aita, D. Antoine, K.R. Arrigo, I. Asanuma, O. Aumont, R. Barber, M. Behrenfeld, R. Bidigare, E.T. Buitenhuis, J. Campbell, A. Ciotti, H. Dierssen, M. Dowell, J. Dunne, W. Esaias, B. Gentili, W. Gregg, S. Groom, N. Hoepffner, J. Ishizaka, T. Kameda, C. Le Quéré, S. Lohrenz, J. Marra, F. Mélin, K. Moore, A. Morel, T.E. Reddy, J. Ryan, M. Scardi, T. Smyth, K. Turpie, G. Tilstone, K. Waters, and Y. Yamanaka, 2006: A comparison of global estimates of marine primary production from ocean color. *Deep Sea Research Part II: Topical Studies in Oceanography,* **53,** 741-770. http://dx.doi.org/10.1016/j.dsr2.2006.01.028

Carslaw, K.S., L.A. Lee, C.L. Reddington, K.J. Pringle, A. Rap, P.M. Forster, G.W. Mann, D.V. Spracklen, M.T. Woodhouse, L.A. Regayre, and J.R. Pierce, 2013: Large contribution of natural aerosols to uncertainty in indirect forcing. *Nature,* **503,** 67-71. http://dx.doi.org/10.1038/nature12674

Chavez, F.P., M. Messié, and J.T. Pennington, 2011: Marine primary production in relation to climate variability and change. *Annual Review of Marine Science,* **3,** 227-260. http://dx.doi.org/10.1146/annurev.marine.010908.163917

Chen, T., W.B. Rossow, and Y. Zhang, 2000: Radiative effects of cloud-type variations. *Journal of Climate,* **13,** 264-286. http://dx.doi.org/10.1175/1520-0442(2000)013<0264:reoctv>2.0.co;2

Chin, M., T. Diehl, Q. Tan, J.M. Prospero, R.A. Kahn, L.A. Remer, H. Yu, A.M. Sayer, H. Bian, I.V. Geogdzhayev, B.N. Holben, S.G. Howell, B.J. Huebert, N.C. Hsu, D. Kim, T.L. Kucsera, R.C. Levy, M.I. Mishchenko, X. Pan, P.K. Quinn, G.L. Schuster, D.G. Streets, S.A. Strode, O. Torres, and X.P. Zhao, 2014: Multi-decadal aerosol variations from 1980 to 2009: A perspective from observations and a global model. *Atmospheric Chemistry and Physics,* **14,** 3657-3690. http://dx.doi.org/10.5194/acp-14-3657-2014

FINAL DRAFT

Chiodo, G., D.R. Marsh, R. Garcia-Herrera, N. Calvo, and J.A. García, 2014: On the detection of the solar signal in the tropical stratosphere. *Atmospheric Chemistry and Physics,* **14,** 5251-5269. http://dx.doi.org/10.5194/acp-14-5251-2014

Ciais, P., C. Sabine, G. Bala, L. Bopp, V. Brovkin, J. Canadell, A. Chhabra, R. DeFries, J. Galloway, M. Heimann, C. Jones, C. Le Quéré, R.B. Myneni, S. Piao, and P. Thornton, 2013: Carbon and other biogeochemical cycles. *Climate Change 2013: The Physical Science Basis. Contribution of Working Group I to the Fifth Assessment Report of the Intergovernmental Panel on Climate Change*. Stocker, T.F., D. Qin, G.-K. Plattner, M. Tignor, S.K. Allen, J. Boschung, A. Nauels, Y. Xia, V. Bex, and P.M. Midgley, Eds. Cambridge University Press, Cambridge, United Kingdom and New York, NY, USA, 465–570. http://www.climatechange2013.org/report/full-report/

Clark, P.U., J.D. Shakun, S.A. Marcott, A.C. Mix, M. Eby, S. Kulp, A. Levermann, G.A. Milne, P.L. Pfister, B.D. Santer, D.P. Schrag, S. Solomon, T.F. Stocker, B.H. Strauss, A.J. Weaver, R. Winkelmann, D. Archer, E. Bard, A. Goldner, K. Lambeck, R.T. Pierrehumbert, and G.-K. Plattner, 2016: Consequences of twenty-first-century policy for multi-millennial climate and sea-level change. *Nature Climate Change,* **6,** 360-369. http://dx.doi.org/10.1038/nclimate2923

Collins, M., R. Knutti, J. Arblaster, J.-L. Dufresne, T. Fichefet, P. Friedlingstein, X. Gao, W.J. Gutowski, T. Johns, G. Krinner, M. Shongwe, C. Tebaldi, A.J. Weaver, and M. Wehner, 2013: Long-term climate change: Projections, commitments and irreversibility. *Climate Change 2013: The Physical Science Basis. Contribution of Working Group I to the Fifth Assessment Report of the Intergovernmental Panel on Climate Change*. Stocker, T.F., D. Qin, G.-K. Plattner, M. Tignor, S.K. Allen, J. Boschung, A. Nauels, Y. Xia, V. Bex, and P.M. Midgley, Eds. Cambridge University Press, Cambridge, United Kingdom and New York, NY, USA, 1029–1136. http://www.climatechange2013.org/report/full-report/

Cook, B.I., S.P. Shukla, M.J. Puma, and L.S. Nazarenko, 2015: Irrigation as an historical climate forcing. *Climate Dynamics,* **44,** 1715-1730. http://dx.doi.org/10.1007/s00382-014-2204-7

Crook, J.A. and P.M. Forster, 2011: A balance between radiative forcing and climate feedback in the modeled 20th century temperature response. *Journal of Geophysical Research: Atmospheres,* **116,** n/a-n/a. http://dx.doi.org/10.1029/2011JD015924

Davies, J.H. and D.R. Davies, 2010: Earth's surface heat flux. *Solid Earth,* **1,** 5-24. http://dx.doi.org/10.5194/se-1-5-2010

Dentener, F., D. Stevenson, J. Cofala, R. Mechler, M. Amann, P. Bergamaschi, F. Raes, and R. Derwent, 2005: The impact of air pollutant and methane emission controls on tropospheric ozone and radiative forcing: CTM calculations for the period 1990-2030. *Atmospheric Chemistry and Physics,* **5,** 1731-1755. http://dx.doi.org/10.5194/acp-5-1731-2005

FINAL DRAFT

Dessler, A.E., M.R. Schoeberl, T. Wang, S.M. Davis, K.H. Rosenlof, and J.P. Vernier, 2014: Variations of stratospheric water vapor over the past three decades. *Journal of Geophysical Research: Atmospheres,* **119,** 12,588-12,598. http://dx.doi.org/10.1002/2014JD021712

Dhomse, S.S., M.P. Chipperfield, W. Feng, W.T. Ball, Y.C. Unruh, J.D. Haigh, N.A. Krivova, S.K. Solanki, and A.K. Smith, 2013: Stratospheric O_3 changes during 2001–2010: The small role of solar flux variations in a chemical transport model. *Atmospheric Chemistry and Physics,* **13,** 10113-10123. http://dx.doi.org/10.5194/acp-13-10113-2013

Dietmüller, S., M. Ponater, and R. Sausen, 2014: Interactive ozone induces a negative feedback in CO2-driven climate change simulations. *Journal of Geophysical Research: Atmospheres,* **119,** 1796-1805. http://dx.doi.org/10.1002/2013JD020575

Doney, S.C., 2010: The growing human footprint on coastal and open-ocean biogeochemistry. *Science,* **328,** 1512-6. http://dx.doi.org/10.1126/science.1185198

Durack, P.J. and S.E. Wijffels, 2010: Fifty-year trends in global ocean salinities and their relationship to broad-scale warming. *Journal of Climate,* **23,** 4342-4362. http://dx.doi.org/10.1175/2010jcli3377.1

Enderlin, E.M. and G.S. Hamilton, 2014: Estimates of iceberg submarine melting from high-resolution digital elevation models: Application to Sermilik Fjord, East Greenland. *Journal of Glaciology,* **60,** 1084-1092. http://dx.doi.org/10.3189/2014JoG14J085

Ermolli, I., K. Matthes, T. Dudok de Wit, N.A. Krivova, K. Tourpali, M. Weber, Y.C. Unruh, L. Gray, U. Langematz, P. Pilewskie, E. Rozanov, W. Schmutz, A. Shapiro, S.K. Solanki, and T.N. Woods, 2013: Recent variability of the solar spectral irradiance and its impact on climate modelling. *Atmospheric Chemistry and Physics,* **13,** 3945-3977. http://dx.doi.org/10.5194/acp-13-3945-2013

Falkowski, P.G., M.E. Katz, A.H. Knoll, A. Quigg, J.A. Raven, O. Schofield, and F.J.R. Taylor, 2004: The evolution of modern eukaryotic phytoplankton. *Science,* **305,** 354-360. http://dx.doi.org/10.1126/science.1095964

Fernandes, R., H. Zhao, X. Wang, J. Key, X. Qu, and A. Hall, 2009: Controls on Northern Hemisphere snow albedo feedback quantified using satellite Earth observations. *Geophysical Research Letters,* **36,** L21702. http://dx.doi.org/10.1029/2009GL040057

Fiore, A.M., V. Naik, and E.M. Leibensperger, 2015: Air quality and climate connections. *Journal of the Air & Waste Management Association,* **65,** 645-686. http://dx.doi.org/10.1080/10962247.2015.1040526

Flanner, M.G., 2009: Integrating anthropogenic heat flux with global climate models. *Geophysical Research Letters,* **36,** L02801. http://dx.doi.org/10.1029/2008gl036465

FINAL DRAFT

Flanner, M.G., C.S. Zender, P.G. Hess, N.M. Mahowald, T.H. Painter, V. Ramanathan, and P.J. Rasch, 2009: Springtime warming and reduced snow cover from carbonaceous particles. *Atmospheric Chemistry and Physics,* **9,** 2481-2497. http://dx.doi.org/10.5194/acp-9-2481-2009

Flato, G., J. Marotzke, B. Abiodun, P. Braconnot, S.C. Chou, W. Collins, P. Cox, F. Driouech, S. Emori, V. Eyring, C. Forest, P. Gleckler, E. Guilyardi, C. Jakob, V. Kattsov, C. Reason, and M. Rummukainen, 2013: Evaluation of climate models. *Climate Change 2013: The Physical Science Basis. Contribution of Working Group I to the Fifth Assessment Report of the Intergovernmental Panel on Climate Change*. Stocker, T.F., D. Qin, G.-K. Plattner, M. Tignor, S.K. Allen, J. Boschung, A. Nauels, Y. Xia, V. Bex, and P.M. Midgley, Eds. Cambridge University Press, Cambridge, United Kingdom and New York, NY, USA, 741–866. http://www.climatechange2013.org/report/full-report/

Floyd, L.E., J.W. Cook, L.C. Herring, and P.C. Crane, 2003: SUSIM'S 11-year observational record of the solar UV irradiance. *Advances in Space Research,* **31,** 2111-2120. http://dx.doi.org/10.1016/S0273-1177(03)00148-0

Forster, P., V. Ramaswamy, P. Artaxo, T. Berntsen, R. Betts, D.W. Fahey, J. Haywood, J. Lean, D.C. Lowe, G. Myhre, J. Nganga, R. Prinn, G. Raga, M. Schulz, and R. Van Dorland, 2007: Ch. 2: Changes in atmospheric constituents and in radiative forcing. *Climate Change 2007: The Physical Science Basis. Contribution of Working Group I to the Fourth Assessment Report (AR4) of the Intergovernmental Panel on Climate Change*. Solomon, S., D. Qin, M. Manning, Z. Chen, M. Marquis, K.B. Averyt, M. Tignor, and H.L. Miller, Eds. Cambridge University Press, Cambridge, UK. http://www.ipcc.ch/publications_and_data/ar4/wg1/en/ch2.html

Fowler, D., M. Coyle, U. Skiba, M.A. Sutton, J.N. Cape, S. Reis, L.J. Sheppard, A. Jenkins, B. Grizzetti, J.N. Galloway, P. Vitousek, A. Leach, A.F. Bouwman, K. Butterbach-Bahl, F. Dentener, D. Stevenson, M. Amann, and M. Voss, 2013: The global nitrogen cycle in the twenty-first century. *Philosophical Transactions of the Royal Society B: Biological Sciences,* **368,** 20130164. http://dx.doi.org/10.1098/rstb.2013.0164

Franks, P.J., M.A. Adams, J.S. Amthor, M.M. Barbour, J.A. Berry, D.S. Ellsworth, G.D. Farquhar, O. Ghannoum, J. Lloyd, N. McDowell, R.J. Norby, D.T. Tissue, and S. von Caemmerer, 2013: Sensitivity of plants to changing atmospheric CO2 concentration: From the geological past to the next century. *New Phytologist,* **197,** 1077-1094. http://dx.doi.org/10.1111/nph.12104

Friedlingstein, P., P. Cox, R. Betts, L. Bopp, W.v. Bloh, V. Brovkin, P. Cadule, S. Doney, M. Eby, I. Fung, G. Bala, J. John, C. Jones, F. Joos, T. Kato, M. Kawamiya, W. Knorr, K. Lindsay, H.D. Matthews, T. Raddatz, P. Rayner, C. Reick, E. Roeckner, K.-G. Schnitzler, R. Schnur, K. Strassmann, A.J. Weaver, C. Yoshikawa, and N. Zeng, 2006: Climate–carbon

FINAL DRAFT

cycle feedback analysis: Results from the C4MIP model intercomparison. *Journal of Climate,* **19,** 3337-3353. http://dx.doi.org/10.1175/JCLI3800.1

Friedlingstein, P., M. Meinshausen, V.K. Arora, C.D. Jones, A. Anav, S.K. Liddicoat, and R. Knutti, 2014: Uncertainties in CMIP5 climate projections due to carbon cycle feedbacks. *Journal of Climate,* **27,** 511-526. http://dx.doi.org/10.1175/JCLI-D-12-00579.1

Fröhlich, C. and J. Lean, 2004: Solar radiative output and its variability: Evidence and mechanisms. *The Astronomy and Astrophysics Review,* **12,** 273-320. http://dx.doi.org/10.1007/s00159-004-0024-1

Frölicher, T.L., K.B. Rodgers, C.A. Stock, and W.W.L. Cheung, 2016: Sources of uncertainties in 21st century projections of potential ocean ecosystem stressors. *Global Biogeochemical Cycles,* **30,** 1224-1243. http://dx.doi.org/10.1002/2015GB005338

Fu, W., J.T. Randerson, and J.K. Moore, 2016: Climate change impacts on net primary production (NPP) and export production (EP) regulated by increasing stratification and phytoplankton community structure in the CMIP5 models. *Biogeosciences,* **13,** 5151-5170. http://dx.doi.org/10.5194/bg-13-5151-2016

Gao, F.-L., L.-R. Tao, G.-M. Cui, J.-L. Xu, and T.-C. Hua, 2015: The influence of solar spectral variations on global radiative balance. *Advances in Space Research,* **55,** 682-687. http://dx.doi.org/10.1016/j.asr.2014.10.028

Gelderloos, R., F. Straneo, and C.A. Katsman, 2012: Mechanisms behind the temporary shutdown of deep convection in the Labrador Sea: Lessons from the great salinity anomaly years 1968–71. *Journal of Climate,* **25,** 6743-6755. http://dx.doi.org/10.1175/jcli-d-11-00549.1

Gerlach, T., 2011: Volcanic versus anthropogenic carbon dioxide. *Eos, Transactions, American Geophysical Union,* **92,** 201-202. http://dx.doi.org/10.1029/2011EO240001

Gillett, N.P., M.F. Wehner, S.F.B. Tett, and A.J. Weaver, 2004: Testing the linearity of the response to combined greenhouse gas and sulfate aerosol forcing. *Geophysical Research Letters,* **31,** L14201. http://dx.doi.org/10.1029/2004GL020111

González-Eguino, M. and M.B. Neumann, 2016: Significant implications of permafrost thawing for climate change control. *Climatic Change,* **136,** 381-388. http://dx.doi.org/10.1007/s10584-016-1666-5

Good, P., J.M. Gregory, J.A. Lowe, and T. Andrews, 2013: Abrupt CO2 experiments as tools for predicting and understanding CMIP5 representative concentration pathway projections. *Climate Dynamics,* **40,** 1041-1053. http://dx.doi.org/10.1007/s00382-012-1410-4

FINAL DRAFT

Gray, L.J., J. Beer, M. Geller, J.D. Haigh, M. Lockwood, K. Matthes, U. Cubasch, D. Fleitmann, G. Harrison, L. Hood, J. Luterbacher, G.A. Meehl, D. Shindell, B. van Geel, and W. White, 2010: Solar influences on climate. *Reviews of Geophysics,* **48,** RG4001. http://dx.doi.org/10.1029/2009RG000282

Hall, A., 2004: The role of surface albedo feedback in climate. *Journal of Climate,* **17,** 1550-1568. http://dx.doi.org/10.1175/1520-0442(2004)017<1550:TROSAF>2.0.CO;2

Hall, A. and X. Qu, 2006: Using the current seasonal cycle to constrain snow albedo feedback in future climate change. *Geophysical Research Letters,* **33,** L03502. http://dx.doi.org/10.1029/2005GL025127

Han, Z., J. Li, W. Guo, Z. Xiong, and W. Zhang, 2013: A study of dust radiative feedback on dust cycle and meteorology over East Asia by a coupled regional climate-chemistry-aerosol model. *Atmospheric Environment,* **68,** 54-63. http://dx.doi.org/10.1016/j.atmosenv.2012.11.032

Hansen, J. and L. Nazarenko, 2004: Soot climate forcing via snow and ice albedos. *Proceedings of the National Academy of Sciences of the United States of America,* **101,** 423-428. http://dx.doi.org/10.1073/pnas.2237157100

Hartmann, D.L., M.E. Ockert-Bell, and M.L. Michelsen, 1992: The effect of cloud type on Earth's energy balance: Global analysis. *Journal of Climate,* **5,** 1281-1304. http://dx.doi.org/10.1175/1520-0442(1992)005<1281:teocto>2.0.co;2

Hartmann, D.L., A.M.G. Klein Tank, M. Rusticucci, L.V. Alexander, S. Brönnimann, Y. Charabi, F.J. Dentener, E.J. Dlugokencky, D.R. Easterling, A. Kaplan, B.J. Soden, P.W. Thorne, M. Wild, and P.M. Zhai, 2013: Observations: Atmosphere and surface. *Climate Change 2013: The Physical Science Basis. Contribution of Working Group I to the Fifth Assessment Report of the Intergovernmental Panel on Climate Change*. Stocker, T.F., D. Qin, G.-K. Plattner, M. Tignor, S.K. Allen, J. Boschung, A. Nauels, Y. Xia, V. Bex, and P.M. Midgley, Eds. Cambridge University Press, Cambridge, United Kingdom and New York, NY, USA, 159–254. http://www.climatechange2013.org/report/full-report/

Hauglustaine, D.A., J. Lathière, S. Szopa, and G.A. Folberth, 2005: Future tropospheric ozone simulated with a climate-chemistry-biosphere model. *Geophysical Research Letters,* **32,** L24807. http://dx.doi.org/10.1029/2005GL024031

Hegglin, M.I., D.A. Plummer, T.G. Shepherd, J.F. Scinocca, J. Anderson, L. Froidevaux, B. Funke, D. Hurst, A. Rozanov, J. Urban, T. von Clarmann, K.A. Walker, H.J. Wang, S. Tegtmeier, and K. Weigel, 2014: Vertical structure of stratospheric water vapour trends derived from merged satellite data. *Nature Geoscience,* **7,** 768-776. http://dx.doi.org/10.1038/ngeo2236

FINAL DRAFT

Held, I.M. and B.J. Soden, 2000: Water vapor feedback and global warming. *Annual Review of Energy and the Environment,* **25,** 441-475. http://dx.doi.org/10.1146/annurev.energy.25.1.441

Hibbard, K.A., G.A. Meehl, P.M. Cox, and P. Friedlingstein, 2007: A strategy for climate change stabilization experiments. *Eos, Transactions, American Geophysical Union,* **88,** 217-221. http://dx.doi.org/10.1029/2007EO200002

Holland, D.M., R.H. Thomas, B. de Young, M.H. Ribergaard, and B. Lyberth, 2008: Acceleration of Jakobshavn Isbrae triggered by warm subsurface ocean waters. *Nature Geoscience,* **1,** 659-664. http://dx.doi.org/10.1038/ngeo316

Holmes, C.D., M.J. Prather, O.A. Søvde, and G. Myhre, 2013: Future methane, hydroxyl, and their uncertainties: Key climate and emission parameters for future predictions. *Atmospheric Chemistry and Physics,* **13,** 285-302. http://dx.doi.org/10.5194/acp-13-285-2013

Hsu, N.C., R. Gautam, A.M. Sayer, C. Bettenhausen, C. Li, M.J. Jeong, S.C. Tsay, and B.N. Holben, 2012: Global and regional trends of aerosol optical depth over land and ocean using SeaWiFS measurements from 1997 to 2010. *Atmospheric Chemistry and Physics,* **12,** 8037-8053. http://dx.doi.org/10.5194/acp-12-8037-2012

IPCC, 2007: *Climate Change 2007: The Physical Science Basis. Contribution of Working Group I to the Fourth Assessment Report of the Intergovernmental Panel on Climate Change*. Solomon, S., D. Qin, M. Manning, Z. Chen, M. Marquis, K.B. Averyt, M. Tignor, and H.L. Miller, Eds. Cambridge University Press, Cambridge. U.K, New York, NY, USA, 996 pp. http://www.ipcc.ch/publications_and_data/publications_ipcc_fourth_assessment_report_wg1_report_the_physical_science_basis.htm

IPCC, 2013: *Climate Change 2013: The Physical Science Basis. Contribution of Working Group I to the Fifth Assessment Report of the Intergovernmental Panel on Climate Change*. Cambridge University Press, Cambridge, UK and New York, NY, 1535 pp. http://www.climatechange2013.org/report/

Isaksen, I., T. Berntsen, S. Dalsøren, K. Eleftheratos, Y. Orsolini, B. Rognerud, F. Stordal, O. Søvde, C. Zerefos, and C. Holmes, 2014: Atmospheric ozone and methane in a changing climate. *Atmosphere,* **5,** 518. http://dx.doi.org/10.3390/atmos5030518

Jacobson, M.Z., 2004: Climate response of fossil fuel and biofuel soot, accounting for soot's feedback to snow and sea ice albedo and emissivity. *Journal of Geophysical Research,* **109,** D21201. http://dx.doi.org/10.1029/2004JD004945

Jiang, X., S.J. Eichelberger, D.L. Hartmann, R. Shia, and Y.L. Yung, 2007: Influence of doubled CO2 on ozone via changes in the Brewer–Dobson circulation. *Journal of the Atmospheric Sciences,* **64,** 2751-2755. http://dx.doi.org/10.1175/jas3969.1

FINAL DRAFT

Jiao, C., M.G. Flanner, Y. Balkanski, S.E. Bauer, N. Bellouin, T.K. Berntsen, H. Bian, K.S. Carslaw, M. Chin, N. De Luca, T. Diehl, S.J. Ghan, T. Iversen, A. Kirkevåg, D. Koch, X. Liu, G.W. Mann, J.E. Penner, G. Pitari, M. Schulz, Ø. Seland, R.B. Skeie, S.D. Steenrod, P. Stier, T. Takemura, K. Tsigaridis, T. van Noije, Y. Yun, and K. Zhang, 2014: An AeroCom assessment of black carbon in Arctic snow and sea ice. *Atmospheric Chemistry and Physics,* **14,** 2399-2417. http://dx.doi.org/10.5194/acp-14-2399-2014

Jin, X., N. Gruber, J.P. Dunne, J.L. Sarmiento, and R.A. Armstrong, 2006: Diagnosing the contribution of phytoplankton functional groups to the production and export of particulate organic carbon, CaCO3, and opal from global nutrient and alkalinity distributions. *Global Biogeochemical Cycles,* **20,** GB2015. http://dx.doi.org/10.1029/2005GB002532

John, J.G., A.M. Fiore, V. Naik, L.W. Horowitz, and J.P. Dunne, 2012: Climate versus emission drivers of methane lifetime against loss by tropospheric OH from 1860–2100. *Atmospheric Chemistry and Physics,* **12,** 12021-12036. http://dx.doi.org/10.5194/acp-12-12021-2012

Johnson, G.C., J.M. Lyman, T. Boyer, C.M. Domingues, M. Ishii, R. Killick, D. Monselesan, and S.E. Wijffels, 2016: [Global Oceans] Ocean heat content [in "State of the Climate in 2015"]. *Bulletin of the American Meteorological Society,* **97,** S66-S70. http://dx.doi.org/10.1175/2016BAMSStateoftheClimate.1

Jones, A., J.M. Haywood, and O. Boucher, 2007: Aerosol forcing, climate response and climate sensitivity in the Hadley Centre climate model. *Journal of Geophysical Research,* **112,** D20211. http://dx.doi.org/10.1029/2007JD008688

Joughin, I., R.B. Alley, and D.M. Holland, 2012: Ice-sheet response to oceanic forcing. *Science,* **338,** 1172-1176. http://dx.doi.org/10.1126/science.1226481

Ju, J. and J.G. Masek, 2016: The vegetation greenness trend in Canada and US Alaska from 1984–2012 Landsat data. *Remote Sensing of Environment,* **176,** 1-16. http://dx.doi.org/10.1016/j.rse.2016.01.001

Kay, J.E. and A. Gettelman, 2009: Cloud influence on and response to seasonal Arctic sea ice loss. *Journal of Geophysical Research,* **114,** D18204. http://dx.doi.org/10.1029/2009JD011773

Kay, J.E. and T. L'Ecuyer, 2013: Observational constraints on Arctic Ocean clouds and radiative fluxes during the early 21st century. *Journal of Geophysical Research: Atmospheres,* **118,** 7219-7236. http://dx.doi.org/10.1002/jgrd.50489

Kay, J.E., K. Raeder, A. Gettelman, and J. Anderson, 2011: The boundary layer response to recent Arctic sea ice loss and implications for high-latitude climate feedbacks. *Journal of Climate,* **24,** 428-447. http://dx.doi.org/10.1175/2010JCLI3651.1

FINAL DRAFT

Klocke, D., J. Quaas, and B. Stevens, 2013: Assessment of different metrics for physical climate feedbacks. *Climate Dynamics,* **41,** 1173-1185. http://dx.doi.org/10.1007/s00382-013-1757-1

Knutti, R. and G.C. Hegerl, 2008: The equilibrium sensitivity of the Earth's temperature to radiation changes. *Nature Geoscience,* **1,** 735-743. http://dx.doi.org/10.1038/ngeo337

Knutti, R. and M.A.A. Rugenstein, 2015: Feedbacks, climate sensitivity and the limits of linear models. *Philosophical Transactions of the Royal Society A: Mathematical, Physical and Engineering Sciences,* **373**. http://dx.doi.org/10.1098/rsta.2015.0146

Koffi, B., M. Schulz, F.-M. Bréon, F. Dentener, B.M. Steensen, J. Griesfeller, D. Winker, Y. Balkanski, S.E. Bauer, N. Bellouin, T. Berntsen, H. Bian, M. Chin, T. Diehl, R. Easter, S. Ghan, D.A. Hauglustaine, T. Iversen, A. Kirkevåg, X. Liu, U. Lohmann, G. Myhre, P. Rasch, Ø. Seland, R.B. Skeie, S.D. Steenrod, P. Stier, J. Tackett, T. Takemura, K. Tsigaridis, M.R. Vuolo, J. Yoon, and K. Zhang, 2016: Evaluation of the aerosol vertical distribution in global aerosol models through comparison against CALIOP measurements: AeroCom phase II results. *Journal of Geophysical Research: Atmospheres,* **121,** 7254-7283. http://dx.doi.org/10.1002/2015JD024639

Kopp, G., 2014: An assessment of the solar irradiance record for climate studies. *Journal of Space Weather and Space Climate,* **4,** A14. http://dx.doi.org/10.1051/swsc/2014012

Kopp, G. and J.L. Lean, 2011: A new, lower value of total solar irradiance: Evidence and climate significance. *Geophysical Research Letters,* **38,** L01706. http://dx.doi.org/10.1029/2010GL045777

Kopp, G., N. Krivova, C.J. Wu, and J. Lean, 2016: The impact of the revised sunspot record on solar irradiance reconstructions. *Solar Physics,* **291,** 2951-1965. http://dx.doi.org/10.1007/s11207-016-0853-x

Kostov, Y., K.C. Armour, and J. Marshall, 2014: Impact of the Atlantic meridional overturning circulation on ocean heat storage and transient climate change. *Geophysical Research Letters,* **41,** 2108-2116. http://dx.doi.org/10.1002/2013GL058998

Koven, C.D., E.A.G. Schuur, C. Schädel, T.J. Bohn, E.J. Burke, G. Chen, X. Chen, P. Ciais, G. Grosse, J.W. Harden, D.J. Hayes, G. Hugelius, E.E. Jafarov, G. Krinner, P. Kuhry, D.M. Lawrence, A.H. MacDougall, S.S. Marchenko, A.D. McGuire, S.M. Natali, D.J. Nicolsky, D. Olefeldt, S. Peng, V.E. Romanovsky, K.M. Schaefer, J. Strauss, C.C. Treat, and M. Turetsky, 2015a: A simplified, data-constrained approach to estimate the permafrost carbon–climate feedback. *Philosophical Transactions of the Royal Society A: Mathematical, Physical and Engineering Sciences,* **373**. http://dx.doi.org/10.1098/rsta.2014.0423

Koven, C.D., D.M. Lawrence, and W.J. Riley, 2015b: Permafrost carbon–climate feedback is sensitive to deep soil carbon decomposability but not deep soil nitrogen dynamics.

FINAL DRAFT

Proceedings of the National Academy of Sciences, **112,** 3752-3757. http://dx.doi.org/10.1073/pnas.1415123112

Krishna Moorthy, K., S. Suresh Babu, M.R. Manoj, and S.K. Satheesh, 2013: Buildup of aerosols over the Indian Region. *Geophysical Research Letters,* **40,** 1011-1014. http://dx.doi.org/10.1002/grl.50165

Krissansen-Totton, J. and R. Davies, 2013: Investigation of cosmic ray–cloud connections using MISR. *Geophysical Research Letters,* **40,** 5240-5245. http://dx.doi.org/10.1002/grl.50996

Kühn, T., A.I. Partanen, A. Laakso, Z. Lu, T. Bergman, S. Mikkonen, H. Kokkola, H. Korhonen, P. Räisänen, D.G. Streets, S. Romakkaniemi, and A. Laaksonen, 2014: Climate impacts of changing aerosol emissions since 1996. *Geophysical Research Letters,* **41,** 4711-4718. http://dx.doi.org/10.1002/2014GL060349

Lacis, A.A., G.A. Schmidt, D. Rind, and R.A. Ruedy, 2010: Atmospheric CO_2: Principal control knob governing Earth's temperature. *Science,* **330,** 356-359. http://dx.doi.org/10.1126/science.1190653

Langmann, B., 2014: On the role of climate forcing by volcanic sulphate and volcanic ash. *Advances in Meteorology,* **2014,** 17. http://dx.doi.org/10.1155/2014/340123

Laufkötter, C., M. Vogt, N. Gruber, M. Aita-Noguchi, O. Aumont, L. Bopp, E. Buitenhuis, S.C. Doney, J. Dunne, T. Hashioka, J. Hauck, T. Hirata, J. John, C. Le Quéré, I.D. Lima, H. Nakano, R. Seferian, I. Totterdell, M. Vichi, and C. Völker, 2015: Drivers and uncertainties of future global marine primary production in marine ecosystem models. *Biogeosciences,* **12,** 6955-6984. http://dx.doi.org/10.5194/bg-12-6955-2015

Le Quéré, C., R.M. Andrew, J.G. Canadell, S. Sitch, J.I. Korsbakken, G.P. Peters, A.C. Manning, T.A. Boden, P.P. Tans, R.A. Houghton, R.F. Keeling, S. Alin, O.D. Andrews, P. Anthoni, L. Barbero, L. Bopp, F. Chevallier, L.P. Chini, P. Ciais, K. Currie, C. Delire, S.C. Doney, P. Friedlingstein, T. Gkritzalis, I. Harris, J. Hauck, V. Haverd, M. Hoppema, K. Klein Goldewijk, A.K. Jain, E. Kato, A. Körtzinger, P. Landschützer, N. Lefèvre, A. Lenton, S. Lienert, D. Lombardozzi, J.R. Melton, N. Metzl, F. Millero, P.M.S. Monteiro, D.R. Munro, J.E.M.S. Nabel, S.I. Nakaoka, K. O'Brien, A. Olsen, A.M. Omar, T. Ono, D. Pierrot, B. Poulter, C. Rödenbeck, J. Salisbury, U. Schuster, J. Schwinger, R. Séférian, I. Skjelvan, B.D. Stocker, A.J. Sutton, T. Takahashi, H. Tian, B. Tilbrook, I.T. van der Laan-Luijkx, G.R. van der Werf, N. Viovy, A.P. Walker, A.J. Wiltshire, and S. Zaehle, 2016: Global carbon budget 2016. *Earth System Science Data,* **8,** 605-649. http://dx.doi.org/10.5194/essd-8-605-2016

le Texier, H., S. Solomon, and R.R. Garcia, 1988: The role of molecular hydrogen and methane oxidation in the water vapour budget of the stratosphere. *Quarterly Journal of the Royal Meteorological Society,* **114,** 281-295. http://dx.doi.org/10.1002/qj.49711448002

FINAL DRAFT